Calculating the waveguide invariant (β) by ray-theoretic approaches

Peter Gerstoft, Gerald D'Spain, William A. Kuperman,
and William S. Hodgkiss
Marine Physical Laboratory
University of California San Diego
La Jolla, CA 92093-0238 USA

1

Summary

The waveguide invariant (β) is an efficient approach for predicting broadband ocean acoustic propagation. The background for calculating beta based on a ray theoretic approach is described and theoretical values are found for representative profiles. A numerical approach for calculating beta based on output of a ray tracing code is developed. The approach is demonstrated using two common ray tracing codes: CASS/GRAB and Bellhop.

In the Appendix the MPL installation of the Comprehensive Acoustic System Simulation (CASS) with the Gaussian RAy Bundle (GRAB) Eigenray model is described.

Acknowledgment

This research was supported by the Office of Naval Research, Code 321US, under contract no. N00014-97-D-0350, DO #5.

2 Theory

In a homogeneous range independent wave guide, with medium slowness $s(z)$, a ray is defined uniquely by the ray parameter or horizontal slowness $s_\mathrm{h} = s(z)\cos\theta(z) = s_0\cos\theta_0$ where θ is the angle to horizontal and s_0 and θ_0 are the slowness and launch angle, respectively. The vertical slowness s_v is defined as

$$s_\mathrm{v}(z) = s(z)|\sin\theta(z)| = \sqrt{s^2(z) - s_\mathrm{h}^2} \tag{1}$$

Since the horizontal slowness s_h is constant, the ray angles can be determined from the slownesses

$$|\sin\theta(z)| = \frac{s_\mathrm{v}(z)}{s(z)} = \frac{\sqrt{s^2(z) - s_\mathrm{h}^2}}{s(z)} \qquad |\tan\theta(z)| = \frac{s_\mathrm{v}(z)}{s_\mathrm{h}} = \frac{\sqrt{s^2(z) - s_\mathrm{h}^2}}{s_\mathrm{h}} \tag{2}$$

The cycle range or cycle skip distance is defined as

$$\Lambda = 2\int_{z_\mathrm{l}}^{z_\mathrm{u}} \frac{1}{|\tan\theta(z)|}\mathrm{d}z = 2\int_{z_\mathrm{l}}^{z_\mathrm{u}} \frac{s_\mathrm{h}}{s_\mathrm{v}(z)}\mathrm{d}z \tag{3}$$

and the corresponding ray cycle time

$$T = 2\int_{z_\mathrm{l}}^{z_\mathrm{u}} \frac{s(z)}{|\sin\theta(z)|}\mathrm{d}z = 2\int_{z_\mathrm{l}}^{z_\mathrm{u}} \frac{s^2(z)}{s_\mathrm{v}(z)}\mathrm{d}z \tag{4}$$

The ray invariant is given by [1]

$$I = \int_{z_\mathrm{l}}^{z_\mathrm{u}} s_\mathrm{v}(z)\mathrm{d}z = \int_{z_\mathrm{l}}^{z_\mathrm{u}} \sqrt{s^2(z) - s_\mathrm{h}^2}\mathrm{d}z \tag{5}$$

The upper and lower bounds (z_u and z_l) are found as the limits to where $s_\mathrm{v} = 0$ or the maximum extend of the waveguide. As seen from the above equation, the ray invariant is the depth-integrated vertical slowness.

Based on the above definitions for Λ, T and I the following expressions are obtained

$$2I = T - s_\mathrm{h}\Lambda \tag{6}$$

$$\frac{\partial T}{\partial s_\mathrm{h}} = s_\mathrm{h}\frac{\partial \Lambda}{\partial s_\mathrm{h}} \tag{7}$$

$$\frac{\partial 2I}{\partial s_\mathrm{h}} = -\Lambda \tag{8}$$

For a ray theoretic point of view the horizontal group slowness [1] is given by

$$s_{\mathrm{g}} = \frac{T}{\Lambda} \tag{9}$$

The waveguide invariant β [1, 2] is defined as

$$\beta^{-1} = -\frac{\partial s_{\mathrm{g}}}{\partial s_{\mathrm{h}}} \tag{10}$$

Based on the equations defined above, several expressions can be defined for β^{-1}

$$\begin{aligned}
\beta^{-1} &= -\left(\frac{\partial T}{\Lambda \partial s_{\mathrm{h}}} - \frac{T \partial \Lambda}{\Lambda^2 \partial s_{\mathrm{h}}}\right) && (11)\\
&= \frac{2I}{\Lambda^2}\frac{\partial \Lambda}{\partial s_{\mathrm{h}}} && (12)\\
&= -2I\frac{\partial \frac{1}{\Lambda}}{\partial s_{\mathrm{h}}} && (13)\\
&= -2I\sin\theta_0\frac{\partial \frac{1}{\Lambda}}{\partial \theta_0} && (14)\\
&= -\frac{\partial \Lambda}{\Lambda \partial \theta_0}\frac{I \partial \theta_0}{\partial I} && (15)
\end{aligned}$$

For evaluation of Eq. (12), the following integral can be derived from Eq. (3)

$$\frac{\partial \Lambda}{\partial s_{\mathrm{h}}} = 2\int_{z_{\mathrm{l}}}^{z_{\mathrm{u}}} \frac{s^2(z)}{s_{\mathrm{v}}^3(z)}\mathrm{d}z \tag{16}$$

A way to compute β^{-1} is by direct numerical integration and the Eq. (12) seems useful, combined with Eqs. (3, 5, 16). This can be done without any use of a ray tracing code. It should be noted that the three integrands have a singularity for $s_{\mathrm{v}}(z) = 0$. It should, with care, be possible to avoid problems due to this singularity.

In the present approach we have focused on evaluating β^{-1} by use of a ray tracing code for evaluating Λ and evaluating I numerically and then using Eq. (15).

In the next sections, the value of β^{-1} are calculated analytically for a Pekeris waveguide, an n^2 sound speed profile, and a linear sound speed profile. In the analytic approach, we also used Eq. (15) partly for historical reasons and partly because evaluating Eq. (16) analytically is for the present sound speed profiles more complicated.

2.1 Pekeris wave guide

For a Pekeris wave guide the slowness is constant $s(z) = s_0$ and upper and lower boundaries $z_\mathrm{u}, z_\mathrm{l}$, respectively. We obtain

$$\Lambda = 2\int_{z_\mathrm{l}}^{z_\mathrm{u}} \frac{1}{|\tan\theta|}\mathrm{d}z = \frac{2(z_\mathrm{u}-z_\mathrm{l})}{|\tan\theta_0|} \tag{17}$$

$$\frac{\partial\Lambda}{\partial\theta_0} = -\frac{2(z_\mathrm{u}-z_\mathrm{l})\mathrm{sign}(\theta_0)}{\sin^2\theta_0} \tag{18}$$

$$I = \int_{z_\mathrm{l}}^{z_\mathrm{u}} s_\mathrm{v}\mathrm{d}z = (z_\mathrm{u}-z_\mathrm{l})s_0|\sin\theta_0| \tag{19}$$

$$\frac{\partial I}{\partial\theta_0} = (z_\mathrm{u}-z_\mathrm{l})s_0\cos\theta_0\mathrm{sign}(\theta_0) \tag{20}$$

Substituting these equations into Eq. 15 we obtain

$$\beta^{-1} = \frac{1}{\cos^2(\theta_0)} \tag{21}$$

It can be show that this equation will hold approximately for all rays that are reflected at both the upper and lower boundaries. For sufficiently steep angles and assuming a reflecting bottom, all ocean waveguides will approach this formula for steep rays as these rays will be bouncing off both boundaries.

2.2 n^2-linear ssp wave guide

An n^2-linear sound speed profile wave guide with a reflecting surface at $z = 0$ and the source at the surface is investigated. The slowness is given by $s = s_0\sqrt{1-az}$ and $s_\mathrm{v} = s_0\sqrt{\sin^2\theta_0 - az}$. The upper boundary is $z_\mathrm{l} = 0$ and the lower boundary is where the vertical slowness is zero, $z_\mathrm{u} = \frac{1}{a}\sin^2\theta_0$. The following expressions are obtained:

$$\Lambda = 2\int_{z_\mathrm{l}}^{z_\mathrm{u}} \frac{1}{|\tan\theta|}\mathrm{d}z \tag{22}$$

$$= 4\cos\theta_0\int_{z_\mathrm{l}}^{z_\mathrm{u}} \frac{1}{\sqrt{\sin^2\theta_0 - az}}\mathrm{d}z \tag{23}$$

$$= -\frac{4\cos\theta_0}{a}\left[\sqrt{\sin^2\theta_0 - az}\right]_{z_\mathrm{l}}^{z_\mathrm{u}} \tag{24}$$

$$= \frac{4}{a}\cos\theta_0|\sin\theta_0| \tag{25}$$

$$\frac{\partial\Lambda}{\partial\theta_0} = \frac{2}{a}\mathrm{sign}(\theta_0)(\cos^2\theta_0 - \sin^2\theta_0) \tag{26}$$

$$
\begin{aligned}
I &= \int_{z_\mathrm{l}}^{z_\mathrm{u}} s_\mathrm{v}\,\mathrm{d}z && (27)\\
&= s_0 \int_{z_\mathrm{l}}^{z_\mathrm{u}} \sqrt{\sin^2\theta_0 - az}\,\mathrm{d}z && (28)\\
&= -\frac{2s_0}{3a}\left[\sqrt{(\sin^2\theta_0 - az)^3}\right]_{z_\mathrm{l}}^{z_\mathrm{u}} && (29)\\
&= \frac{2s_0}{3a}|\sin^3\theta_0| && (30)\\
\frac{\partial I}{\partial \theta_0} &= \frac{2s_0}{a}\sin^2\theta_0\cos\theta_0 \mathrm{sign}(\theta_0) && (31)
\end{aligned}
$$

Substituting these equations into Eq. 15 we obtain

$$\beta^{-1} = -\frac{1-\tan^2\theta_0}{3} \approx -\frac{1}{3} \tag{32}$$

Note, the formula does not depend on the curvature (a) of the sound speed. For an n^2-linear sound speed symmetric around $z = 0$ the same expression is obtained for β^{-1}

2.3 Linear ssp

A linear sound speed profile with a reflecting surface and source at $z = 0$ is investigated. The slowness is given by $s(z) = s_0\frac{1}{1+gz}$. The vertical slowness is then given by $s_\mathrm{v} = s_0\sqrt{\frac{1}{(1+gz)^2} - \cos^2\theta_0}$ and $z_\mathrm{l} = 0$, $z_\mathrm{u} = \frac{1}{g}(\cos^{-1}\theta_0 - 1)$. In performing the integrations below, the substitution $x = \frac{1}{(1+gz)}$ and thus $\frac{\partial x}{\partial z} = -gx^2$, $x_l = 1, x_u = \cos\theta_0$ is done.

$$
\begin{aligned}
\Lambda &= 2\int_{z_\mathrm{l}}^{z_\mathrm{u}} \frac{1}{\tan\theta}\mathrm{d}z && (33)\\
&= -\frac{2\cos\theta_0}{g}\int_{x_l}^{x_u} \frac{x^{-2}}{\sqrt{x^2 - \cos^2\theta_0}}\mathrm{d}x && (34)\\
&= -\frac{2\cos\theta_0}{g}\left[\frac{\sqrt{x^2-\cos^2\theta_0}}{x^2\cos^2\theta_0}\right]_{x_l}^{x_u} && (35)\\
&= \frac{2\cos\theta_0}{g}\left(|\sin\theta_0| + \cos^2\theta_0 \log\frac{1+\sin\theta_0}{\cos\theta_0}\right) && (36)\\
&= \frac{2|\tan\theta_0|}{g} && (37)\\
& && (38)
\end{aligned}
$$

$$\frac{\partial \Lambda}{\partial \theta_0} = \frac{2}{g}\mathrm{sign}(\theta_0)\cos^{-2}\theta_0 \tag{39}$$

$$I = \int_{z_l}^{z_u} s_v \mathrm{d}z \tag{40}$$

$$= -\frac{s_0}{g}\int_{x_l}^{x_u} \sqrt{x^2-\cos^2\theta_0}\,x^{-2}\mathrm{d}x \tag{41}$$

$$= \frac{s_0}{g}\left[\frac{1}{x}\sqrt{x^2-\cos^2\theta_0} - \log(x+\sqrt{x^2-\cos^2\theta_0})\right]_{x_l}^{x_u} \tag{42}$$

$$= -\frac{s_0}{g}\left(|\sin\theta_0| - H\right) \tag{43}$$

$$\tag{44}$$

$$\frac{\partial I}{\partial \theta_0} = -\frac{s_0}{g}\left(\mathrm{sign}(\theta_0)\cos\theta_0 - \mathrm{sign}(\theta_0)\cos^{-1}(\theta_0)\right) \tag{45}$$

$$= -\frac{s_0}{g}\mathrm{sign}(\theta_0)\left(\cos^2(\theta_0) - 1\right)\right) \tag{46}$$

$$= \frac{s_0}{g}\mathrm{sign}(\theta_0)\frac{\sin^2(\theta_0)}{\cos(\theta_0)} \tag{47}$$

$$\tag{48}$$

where $H = \log\frac{1+|\sin\theta_0|}{\cos\theta_0} = \mathrm{Acosh}(\frac{1}{\cos\theta_0})$

Plugging it all in we obtain

$$\beta^{-1} = -\frac{\partial\Lambda}{\Lambda\partial\theta_0}\frac{I\partial\theta_0}{\partial I} \tag{49}$$

$$= \frac{\mathrm{sign}(\theta_0)}{\cos^2\theta_0|\tan\theta_0|}\frac{|\sin\theta_0| - H}{\mathrm{sign}(\theta_0)\frac{\sin^2(\theta_0)}{\cos(\theta_0)}} \tag{50}$$

$$= \frac{|\sin\theta_0| - H}{|\sin^3(\theta_0)|} \tag{51}$$

Note this expression does not depend on the slope of the sound speed (g). For a sound speed profile symmetric around $z = 0$ the same expression is found for β. For $\theta \approx 0$ the same value of β^{-1} is obtained for a linear sound speed profile as an n^2 profile.

For an arbitrary location of the source, the same formula is obtained as all rays will be reflected at the surface.

2.4 Large angles

For large angles both boundaries will be reflecting and β will approach the one for a shallow water waveguide $\beta = \cos^2(\theta_0)$

3

Beta computed based on output from a ray tracing code

Numerical differentiation is often unstable and using alternative formulas or semi-analytic integration based on sound speed may provide more stable results. Thus a stable approach has been suggested by D'Spain *et al.* [8], where the ocean is modeled as a layered media and in each layer the contribution to the integrals can be solved analytically, this is much more stable. An alternative to this approach is to integrate the simple integrals directly, this approach has, however, not yet been tested.

The following approach is used:

- First run the ray tracing code with the relevant environment. Here, The CASS/GRAB code [4] was used for the ray-tracing, see Appendix A.
- Compute Λ based on a ray-tracing code. This is done by finding where the rays are crossing back over the source depth. Usually two crossings defines the cycle distance, but for a ray with a turning point at the source depth one crossing define the source cycle distance. In order to have a stable estimate the ray should cross several times (say 10). As we are computing Λ based on just one ray-trace output this will not hold for the shallower rays (in a standard environments) and the calculation becomes slightly unstable. The crossing distance also could be found as where it crossed back over the source depth with the same upward/downward direction as the launch angle.
- Compute $\frac{\partial \Lambda}{\partial \theta_0}$ based on direct numerical differentiation. In regions where Λ is not well determined or changes significantly computation of $\frac{\partial \Lambda}{\partial \theta_0}$ will be unstable. This is the most difficult task and it is recommended that in order to obtain stable result $\Delta\theta_0$ must be reasonably large.
- Find upper and lower bound for the integration of I. This becomes slightly unstable if based on the maximum and minimum of the ray-depth from the ray tracing code. Instead it should be found based on where $s_v = 0$.
- Compute I. This is done directly based on numerical integration.
- Compute $\frac{\partial I}{\partial \theta_0}$. This is computed based on numerical differentiation of I. For large changes in I this can be numerically unstable.

4

Validation

The analytic expression and the numerical calculations are compared.

It should be noted that CASS/GRAB internally interpolate the sound speed. Which interpolation is used is not clear, but it is not a linear interpolation. To approximate a linear profile a sound speed point is added for every 1 m. This interpolation causes some instability for $\frac{\partial \Lambda}{\partial \theta}$ when the ray is turning close to an interface there will be a discontinuity in $\frac{\partial \Lambda}{\partial \theta}$ due to the jump in the ray angle at the turning point [8].

In both the validation and the examples it is the calculation of $\frac{\partial \Lambda}{\partial \theta}$ that mostly causes instability.

4.1 Pekeris

The sound speed profile and ray trace for a 120-m deep 1500 m/s Pekeris wave guide with a source at $z = 50$ is shown in Fig. 1 for several launch angles ($\theta_0 = -10, -6.7, -6.6, -0.1°$). The computation of β^{-1} and $I, \Lambda, \frac{\partial I}{\partial \theta_0}, \frac{\partial \Lambda}{\partial \theta_0}$ based on the analytic formulas in Sect. 2.1 (green line) and based on numerical calculations (blue) is shown in Fig. 2. The instability in calculating beta for $|\theta_0| < 2°$ is due to that we only run ray trace once where it is focussed on getting steeper and shorter ranges. Running the ray trace a second time focused on shallow angles and longer ranges could reduce this instability. This applies to all the following calculations of beta.

4.2 Linear sound speed

The sound speed profiles and ray trace for a 120-m deep wave guide with 0.4 m/s/m sloping sound speed profile and source at $z = 50$ is shown in Fig. 3 for launch angles ($\theta_0 = -10, -6.7, -6.6, -0.1°$). The computation of β^{-1} and $I, \Lambda, \frac{\partial I}{\partial \theta_0}, \frac{\partial \Lambda}{\partial \theta_0}$ based on the analytic formulas in Sect. 2.3 (green line) and based on numerical calculations (blue) is shown in Fig. 4. For $|\theta_0| > 14°$ the rays hit the bottom and the propagation pattern then correspond to a reflecting shallow water waveguide.

It is not clear why there is a systematic error between the analytic and the numeric approach in calculating the cycle distance and its derivative. It does not seem very important for the calculation of β^{-1}.

The analytic expression $\beta^{-1} = -\frac{1-\tan^2\theta_0}{3}$ corresponding to the n^2-linear profile is also in the top of Fig. 4. It is seen that the expression for β^{-1} for a linear and an n^2-linear profile are identical for shallow angles, but show small deviations for larger angles.

4.3 n^2 linear sound speed

For this test a 1000-m deep waveguide with sound speed increasing from 1500 m/s to 1450 m/s is investigated with the source at the surface. In order to obtain stable results it was necessary to have the angular increment set to 0.5°.

The result is shown in Fig. 5. It is noted that there is some noise in calculating β, essentially all due to noise in calculating $\frac{\partial\Lambda}{\partial\theta_0}$. the reason for this is a) It is based on interpolation on a discrete grid (here every 10 m in range). b) small errors in the ray tracing can have a large impact on the derivative. c) Jumps in the ray angle for turning points near a discontinuity [8].

5
Examples

The examples are generated for a shallow water waveguide and the source is at 50 m depth. For synthetic examples the bathymetry is 120 m.

For each environment one figure shows the sound speed profile and the ray trace diagram is for selected values of starting angle ($\theta_0 = -10, -6.7, -6.6, -0.1°$). A second figure shows beta and the elements in calculating beta. For reference the $\beta^{-1} = cos^{-2}\theta_0$ for a Pekeris wave guide (red dashed) and $\beta^{-1} = -\frac{1-\tan^2\theta_0}{3}$ corresponding to the n^2-linear profile (green dash-dotted). The elements in calculating beta are $I, \Lambda, \frac{\partial I}{\partial \theta_0}, \frac{\partial \Lambda}{\partial \theta_0}$.

Note that wherever the propagation transitions from one type to another the ray cycle distance reaches an extremum.

The following examples were investigated

1. This example represents a linear sound speed profile in 120-m water, Fig. 6–7. The transition at $|\theta_0| \approx 12°$ is due to the rays being reflected instead of refracted at the bottom. In the refraction region the variation in β^{-1} is the same as with the source at the surface.

2. For a double linear profile with the source on the sound speed axis, Fig. 8–9. There are two transitions in beta as first the surface bounce ($|\theta_0| = 15°$) and then the bottom bounce ($|\theta_0| = 17°$) becomes reflecting. In the refraction region the variation in β^{-1} is the same as a linear sound speed profile.

3. Moving the source off axis for the double linear profiles changes where the transition in refracting/reflecting and beta occurs, for the surface bounce ($|\theta_0| = 12°$) and for bottom bounce ($|\theta_0| = 15°$). In the refraction region the variation in β^{-1} is the same as for a linear sound speed profile.

4. For a trilinear profile, Fig. 12–13 are quite similar to the the previous examples as the upper duct is not important, again transitions are seen for when the surface bounce ($|\theta_0| = 6°$) and then the bottom bounce ($|\theta_0| = 15°$) becomes reflecting. In the pure refraction region the variation in β^{-1} is the same as for a linear sound speed profile.

5. for the n^2-linear profile with the source at 50 m depth, the rays are being reflected for $\theta > 20^\circ$ Fig. 15. Similar to Fig. 5 some instability can be seen in calculating $\frac{\partial \Lambda}{\partial \theta_0}$.

6. For the more realistic SWellEx-96 environment, Fig. 14–17, the values of beta becomes more complicated, though a representative value is $\beta \approx 1$. The transition at $|\theta_0| = 10^\circ$ is drastic and is investigated in further detail in Fig. 14. The change is due to an increase in cycle distance as the surface layer is penetrated and then a decrease as the ray is bouncing off the surface.

7. This example is based on a sound speed profile from the SACLANTCEN MAPEX2K experiment (Nov 2000), Fig. 18–19. The thermocline is here fairly deep (105 m) and the sound speed profile below the thermocline is not important. Thus this environment correspond to a Pekeris waveguide. This is confirmed in Fig. 19. Again the instability for shallow angles can be improved by rerunning the ray tracer with a focus on longer ranges and shallower angles.

8. This example is from the Arctic, Fig. 20. The calculation of β^{-1}, Fig. 21 shows great instability for launch angles around 5°. Due to variation in the cycle distance the derivative $\frac{\partial I}{\partial \theta_0}$ becomes very unstable. This is further investigated in Fig.22, where the cycle distance is maximum for $\theta_0 = -4.7$ and decreases for both a smaller (blue) or larger (red) launch angle.

6

Bellhop

In the previous sections it has been seen that the calculation of β can be sligthly unstable. Part of this unstability can be attributed to the ray theoretic code. To test this we here use the Bellhop code[9]

For testing the 1000-m deep n^2-linear profile with launch angles increments of 0.1 deg is used. (0.5 deg gives stable results, see Fig. 5). With CASS/GRAB we obtained Fig. 23 approximating n^2-linear profile with a sound speed point every 10-m. Using the same sound speed profile as input to Bellhop gave a reduction in the noise, see Fig 24. In bellhop in is possible to use specific sound speed profiles, specifying a n^2-linear profile directly in Bellhop eliminated the noise, see Fig 25.

For horizontal rays β becomes hyper sensitive to small errors in the ray tracing.

Bellhop has several advantages:

- In Bellhop several option for sound speed interpolation is available cubic spline (S), C-linear (C) N2-linear (N) and user supplied (A).
- It is about 50 % faster (we have not done a precise timing).
- It is not a black box, it gives nice output files, and the author is here.
- In the example presented bellhop gave about 50 % less noise than CASS/grab using a discrete sound speed profile. about the same sampling resolution was required. (the noise was eliminated using the analytic N2-linear option in Bellhop).

Bellhop can output the vertical slowness, this can be used for calculating the ray invariant I. We calculate the ray invariant without any ray tracing, as It is often more accurate.

6.1 Derivative of cycle distance

It is not easy (impossible ?) to get stable results with numerical differentiation. In order to get stable derivatives the requirements in the precision of the cycle

distance is extreme. The very small variation in cycle distance for bellhop, Fig. 26, is sufficient to give a noisy appearance in the cycle distance derivative, Fig. 24.

The noise can be reduced by a) increasing $\delta\theta$, b) median filtering [similar to a)], see Fig. 27, c) fitting splines or similar to the cycle distance curve and differentiating these.

The most stable approach is likely to use a dedicated code with analytic integrals in each layer as described in Refspain02.

References

[1] Brekhovskikh, L.M and Y.P. Lysanov *Fundamentals of ocean acoustics* (Spinger-Verlag, 1991).

[2] G.L. D'Spain and W.A. Kuperman "Application of Waveguide invariants to analysis of spectrograms from shallow water environments that vary in range and azimuth," *J. Acoust. Soc. Am.*, vol. 106(5), pp. 2454–2468, Nov. 1999.

[3] G.L. D'Spain and W.A. Kuperman J.J. Murray "Matchless Field Processing in shallow water" *IEEE Oceans-00*, Sept. 2000.

[4] H. Weinberg, R.L. Deavenport, E.H. McCarty and C.M Anderson, "Comprehensive Acoustic System Simulation (CASS) reference guide", NUWC-NPT Technical Reference guide 01-016 (2001)

[5] R.E. Keenan, H. Weinberg, F.E. Aidala, "Software test description: Comprehensive Acoustic System Simulation (CASS), Version 3" CDRL Sequence, Naval Oceanographic Office (2000).

[6] R.E. Keenan, D. Brown, E.H. McCarty, H. Weinberg, L. Gainey and G. Brooke, "Software test description: Comprehensive Acoustic System Simulation (CASS Version 2) with the Gaussian RAy Bundle (GRAB) Eigenray model (GRAB Version 2)" NUWC-NPT Technical Document 11,231 (2000).

[7] R.E. Keenan, H. Weinberg, F.E. Aidala, "Software test description: Gaussian RAy Bundle (GRAB) Eigenray Propagation model, Version 2" CDRL Sequence, Naval Oceanographic Office (2000).

[8] G.L. D'Spain, G. Rovner, P. Gerstoft, W.A. Kuperman, and W.S. Hodgkiss, "Determination of waveguide invariants in general environments," *J. Underwater Acoustics*, submitted, Dec. 2001.

[9] M.B. porter, "The Kraken normal mode model," SACLANTCEN URC, SM-245, 1991

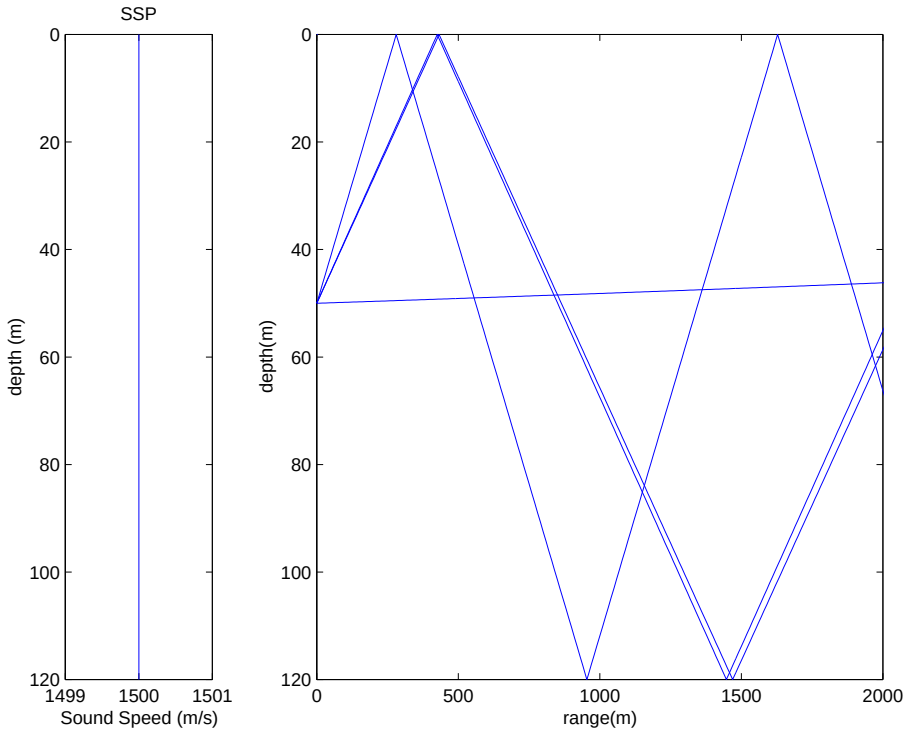

Figure 1 *Sound speed and ray-trace ($\theta_0 = -10, -6.7, -6.6, -0.1^\circ$) for the Pekeris waveguide.* [**pekerisray**]

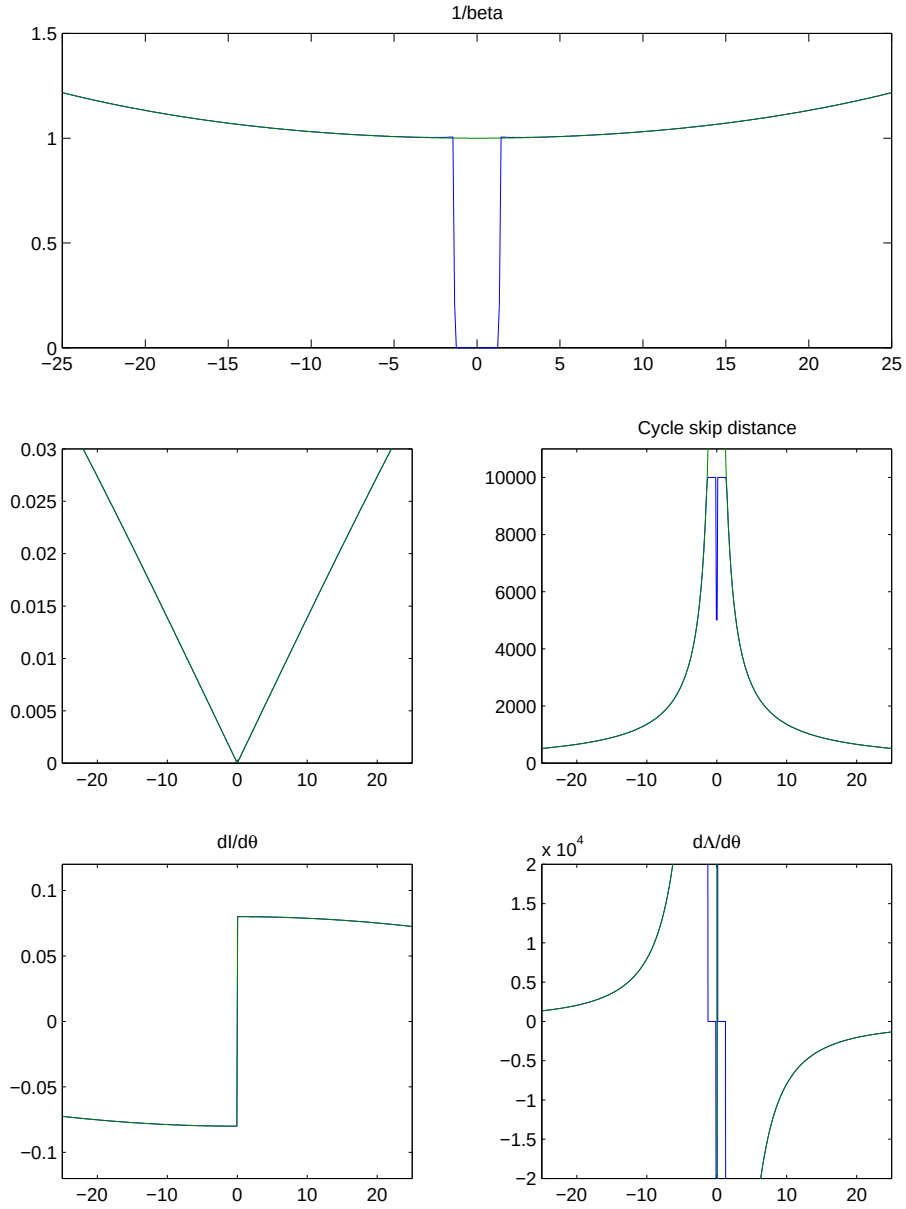

Figure 2 *Beta and related computation for a Pekeris waveguide based on numeric (blue) and analytic (green) approaches. Mostly the green line overlays the blue line.* [**pekerisana**]

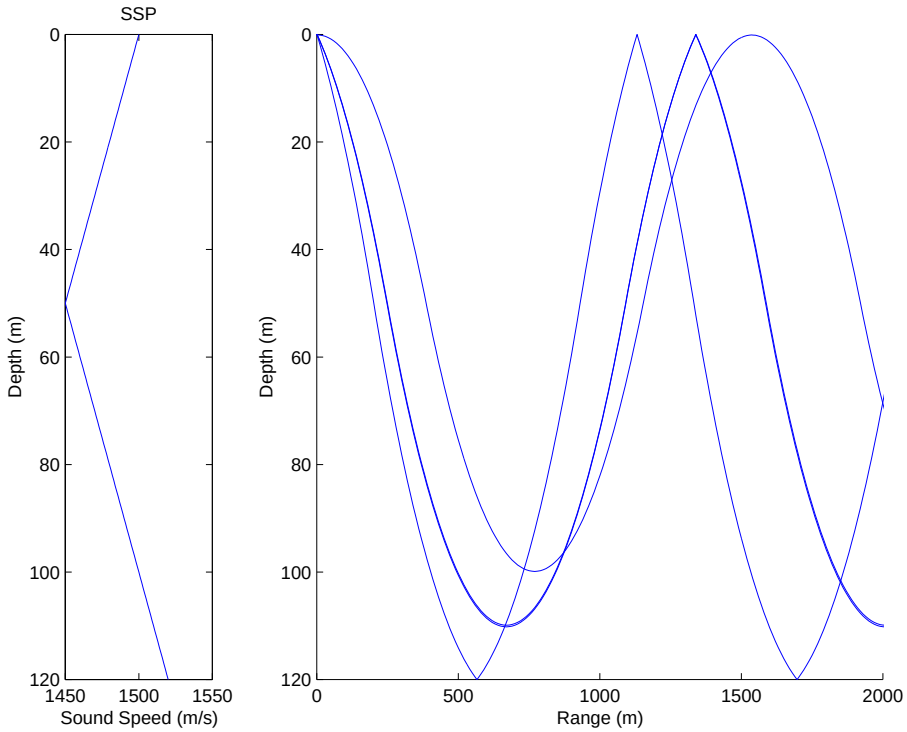

Figure 3 *Sound speed and ray-trace ($\theta_0 = -10, -6.7, -6.6, -0.1°$) for the linear sound speed case. [***slope0ray***]*

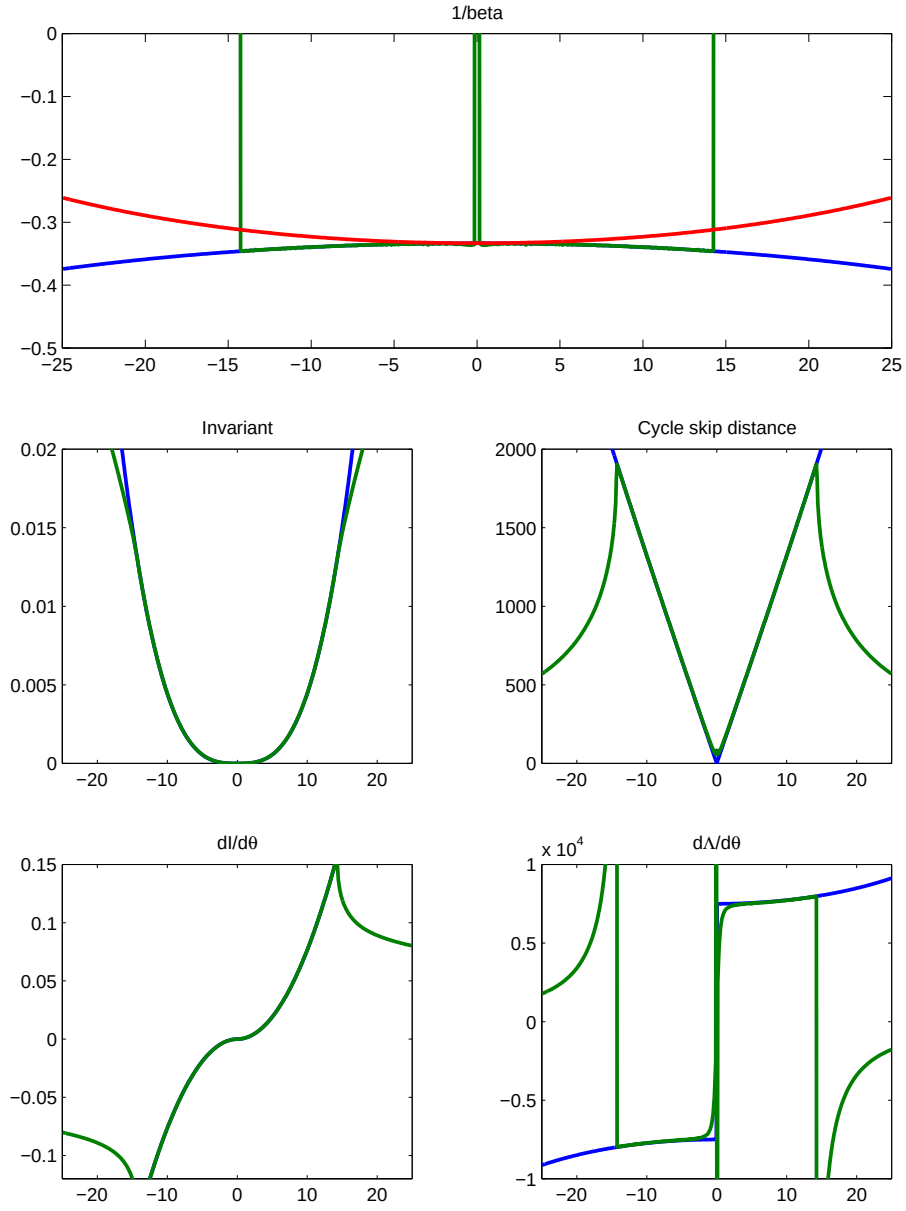

Figure 4 *Computation of β^{-1} for a waveguide with a sound speed profile with a slope of 0.4 m/s/m ($c = 1500 + 0.4z$) based on analytical formulas(blue) and numerical calculations (green). For reference $\beta^{-1} = -\frac{1-\tan^2\theta_0}{3}3$ for n^2 sound speed profile is shown in red. For $|\theta_0| > 11^\circ$ the rays are interacting with both boundaries.* [**slope0ana**]

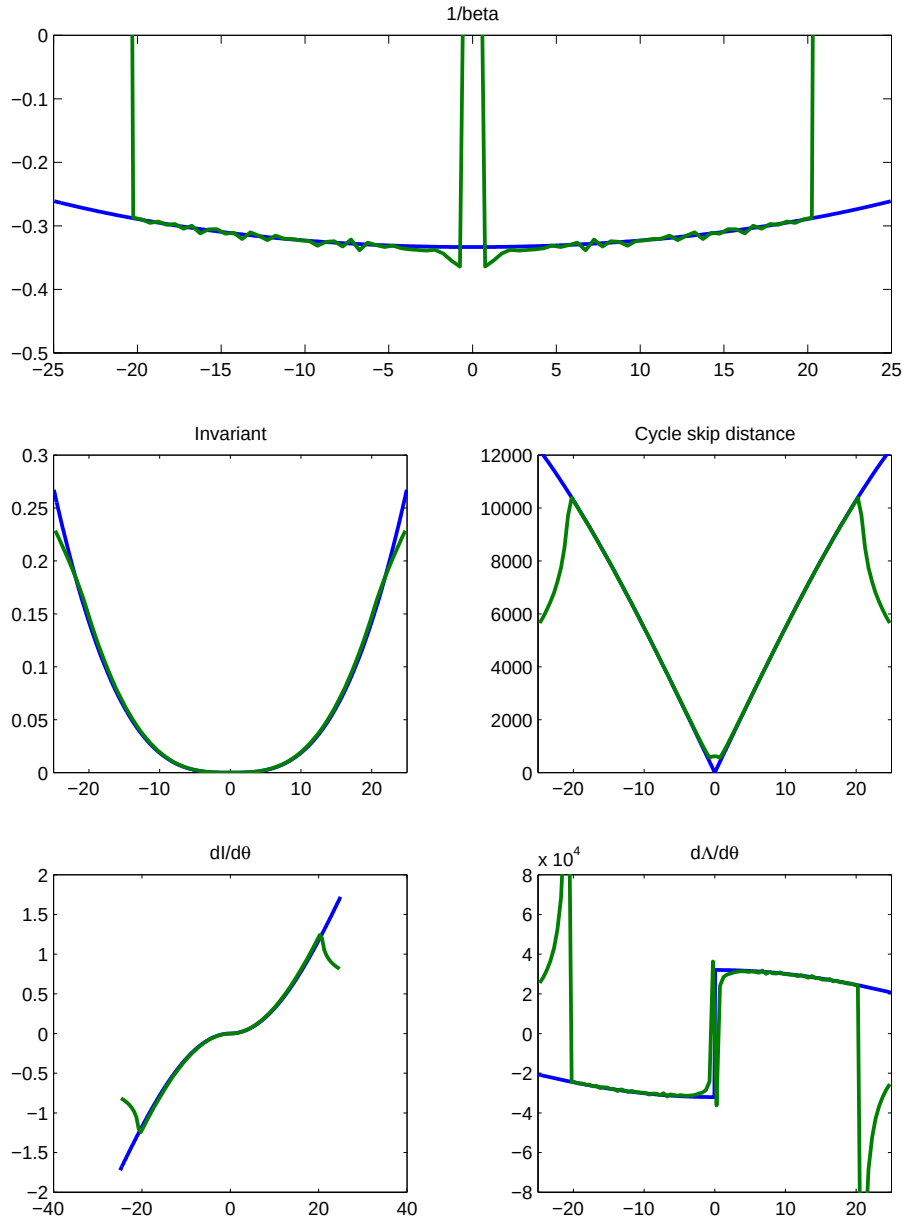

Figure 5 *Computation of β^{-1} for a waveguide with a n^2-linear sound speed varying from 1450 to 1550 m/s based on analytical formulas(blue) and numerical calculations (green). For $|\theta_0| > 20°$ the rays are interacting with both boundaries [***czsqana***]*

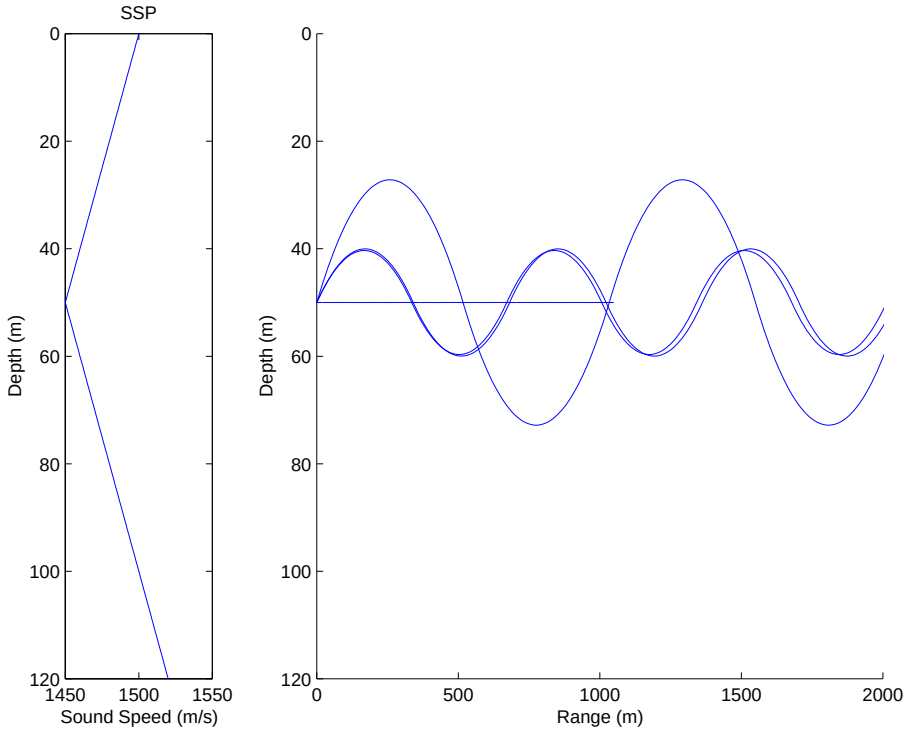

Figure 6 *Sound speed and ray-trace for the slope case. [***sloperay***]*

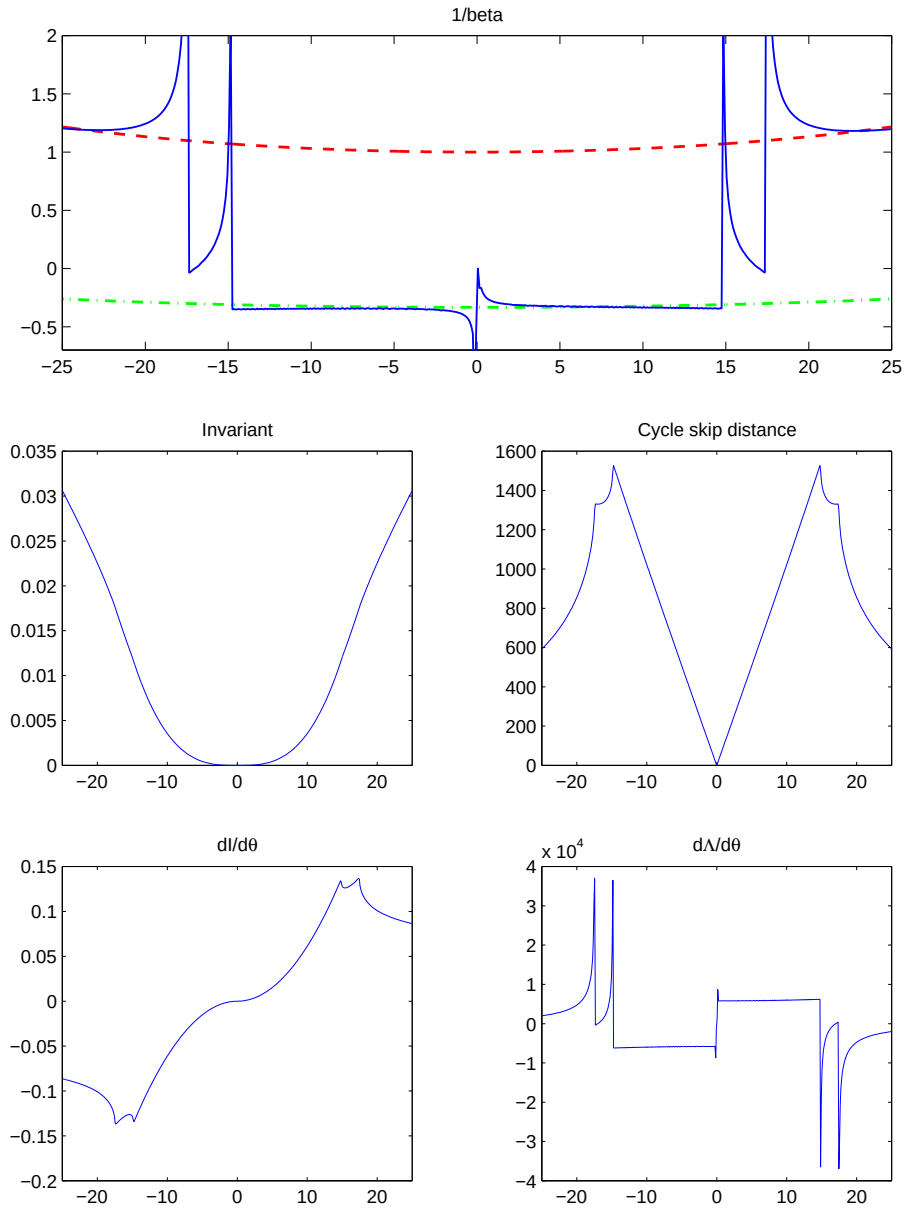

Figure 7 *Beta for a waveguide with a sound speed profile with a slope of 0.4 m/s/m ($c = 1500 + 0.4z$). For reference the $\beta^{-1} = cos^{-2}\theta_0$ for a Pekeris wave guide (red dashed) and $\beta^{-1} = -\frac{1-\tan^2\theta_0}{3}$ corresponding to the n^2-linear profile (green dash-dotted) are shown. For $|\theta_0| > 15°$ the rays are interacting with both boundaries in the numerical approach. [***slope***]*

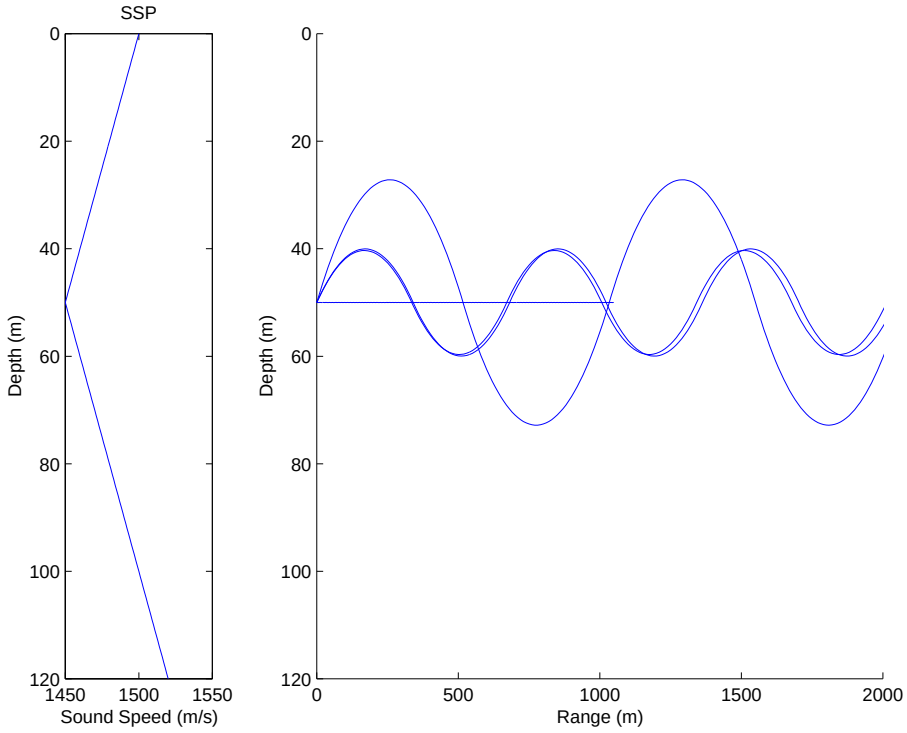

Figure 8 *Sound speed and ray-trace for the double slope case. [***doublesloperay***]*

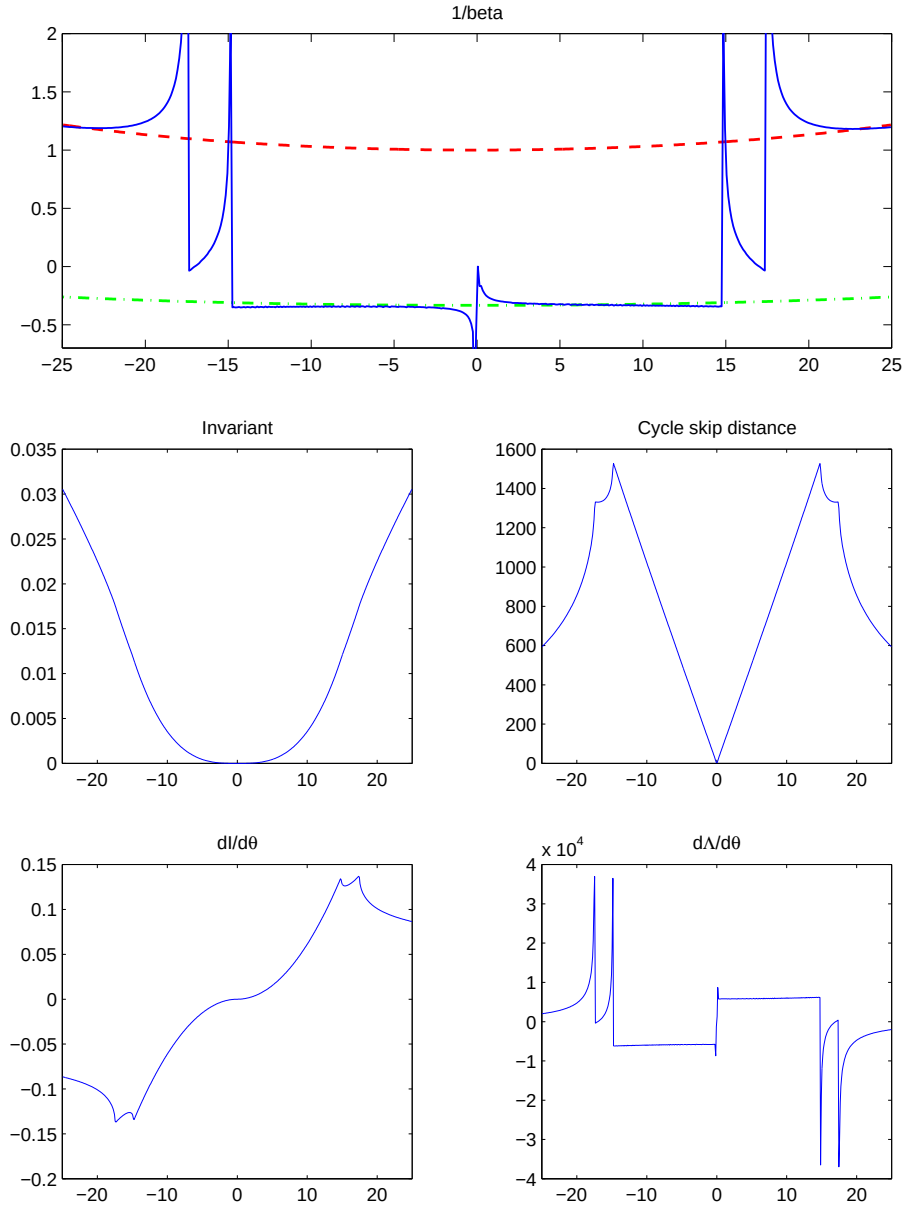

Figure 9 *Beta for a waveguide with a trapping sound speed profile. The sound speed varies linearly from 1500 m/s at the top to 1450 at the source (50 m) to 1520m/s at the bottom. For reference the* $\beta^{-1} = cos^{-2}\theta_0$ *for a Pekeris wave guide (red dashed) and* $\beta^{-1} = -\frac{1-\tan^2\theta_0}{3}$ *corresponding to the* n^2*-linear profile (green dash-dotted) are shown. The results are much more stable than the single slope case.* [**doubleslope**]

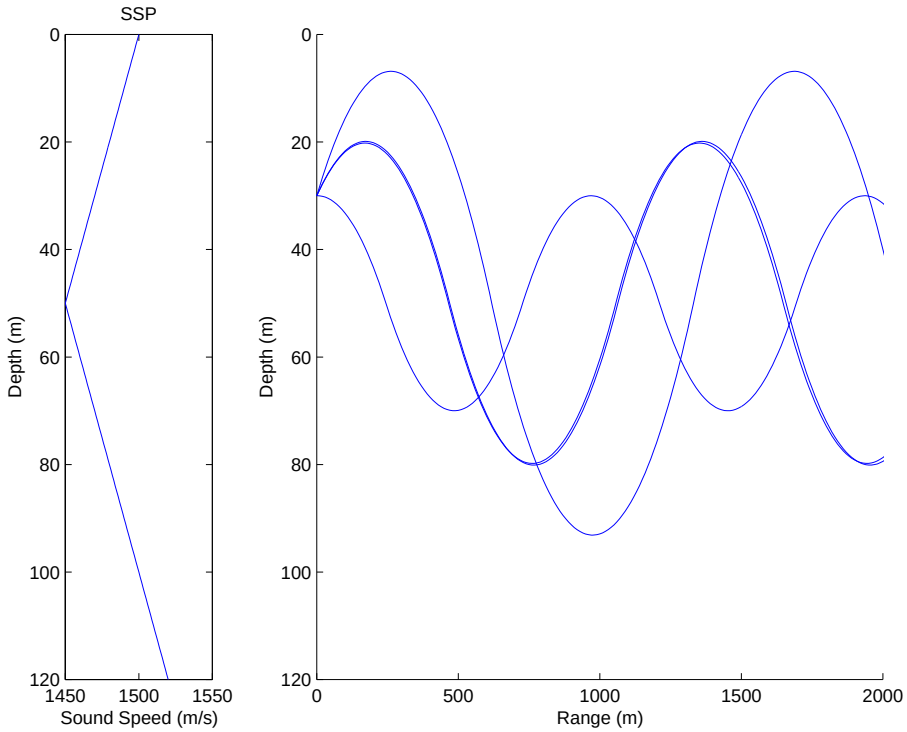

Figure 10 *Sound speed and ray-trace for the double slope case.* [**doubleslope30ray**]

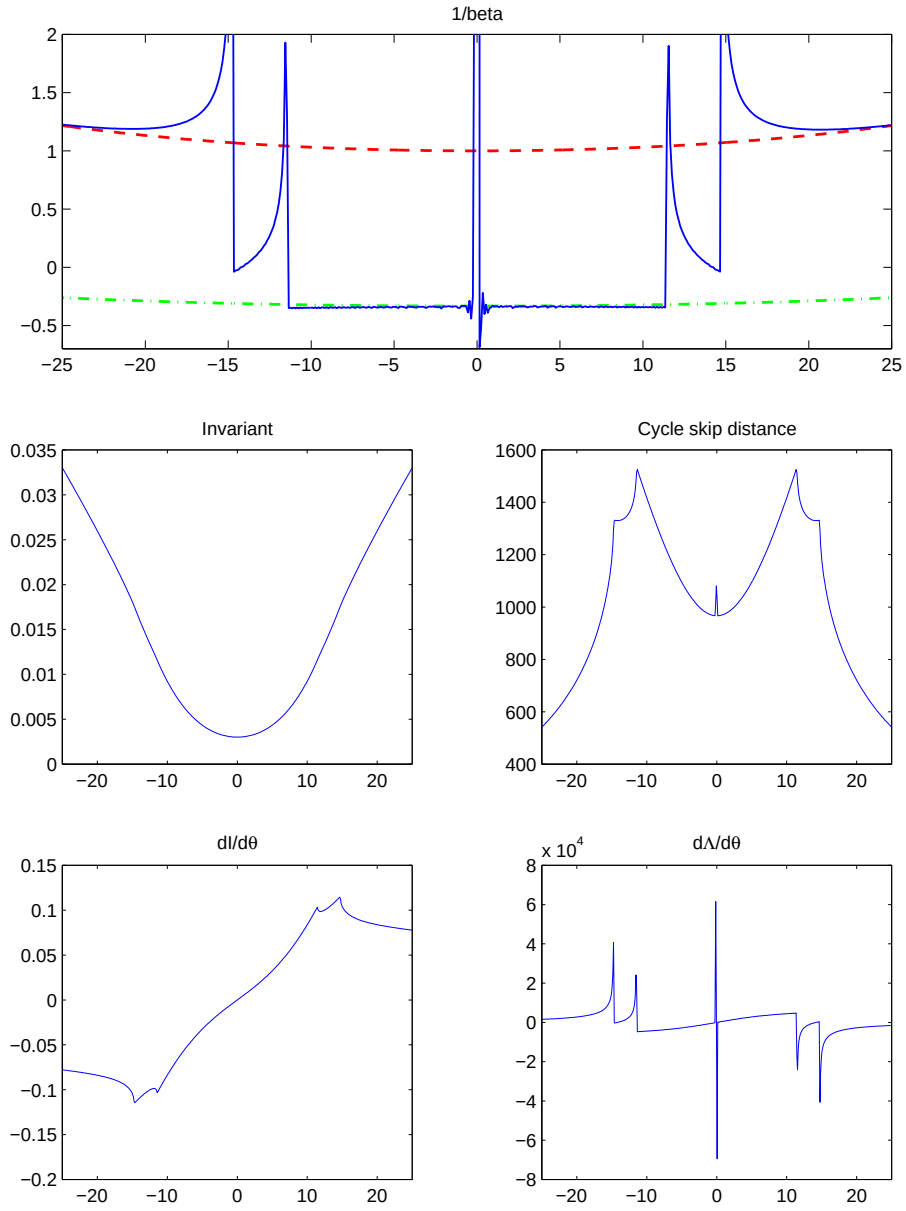

Figure 11 *Beta for a waveguide with a trapping sound speed profile, the source is at 30 m depth. The sound speed varies linearly from 1500 m/s at the top to 1450 at 50 m to 1520m/s at the bottom. For reference the* $\beta^{-1} = cos^{-2}\theta_0$ *for a Pekeris wave guide (red dashed) and* $\beta^{-1} = -\frac{1-\tan^2\theta_0}{3}$ *corresponding to the* n^2*-linear profile (green dash-dotted) are shown. The results are much more stable than the single slope case.* [**doubleslope30**]

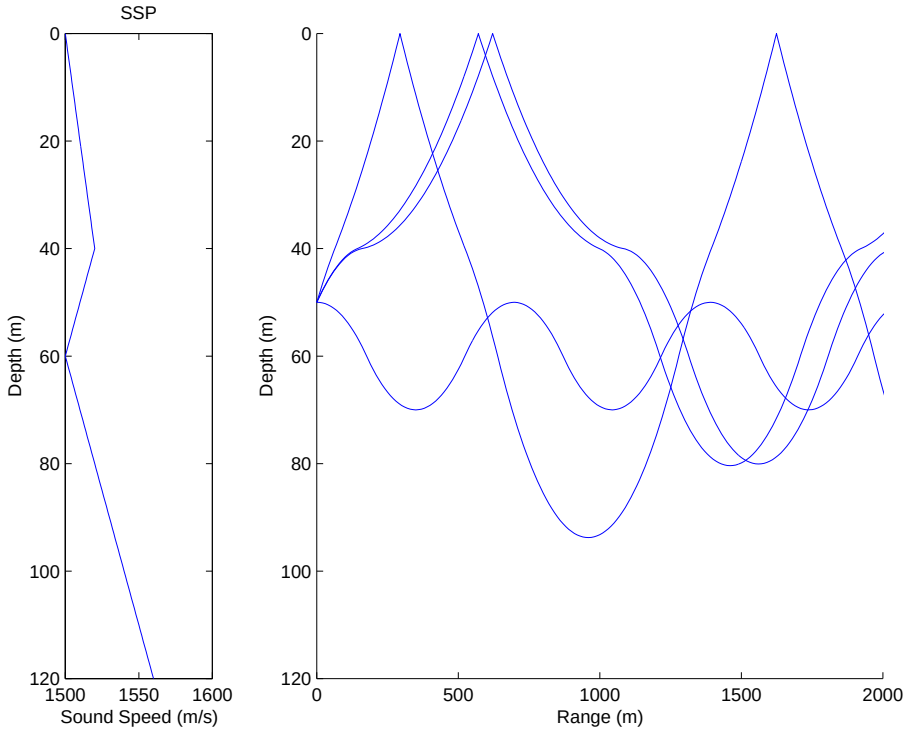

Figure 12 *Sound speed and ray trace for the double duct case for* $\theta_0 = -10, -6.7, -6.6, -0.1\,\mathrm{deg}$. *Note the huge difference when* θ_0 *changes from* -6.7 *to* -6.6. *The cycle distance changes a factor two. [***doubleductray***]*

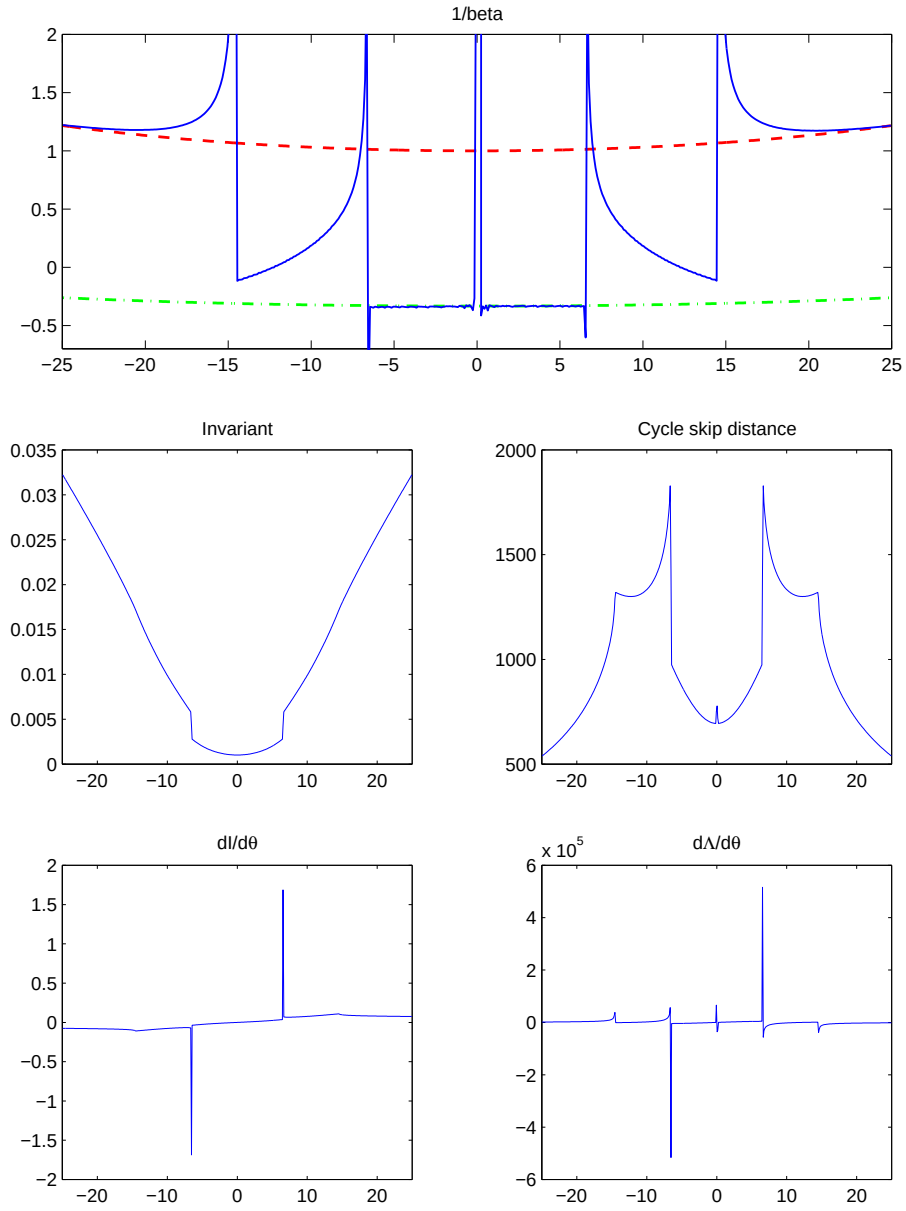

Figure 13 *Beta for a waveguide with a trapping sound speed profile, the source is at 50 m depth. The sound speed varies linearly from (0m ,1500 m/s) (40, 1520),(60,15000, (120, 1560). For reference the* $\beta^{-1} = cos^{-2}\theta_0$ *for a Pekeris wave guide (red dashed) and* $\beta^{-1} = -\frac{1-\tan^2\theta_0}{3}$ *corresponding to the* n^2*-linear profile (green dash-dotted) are shown. The results are much more stable than the single slope case.* [**doubleduct**]

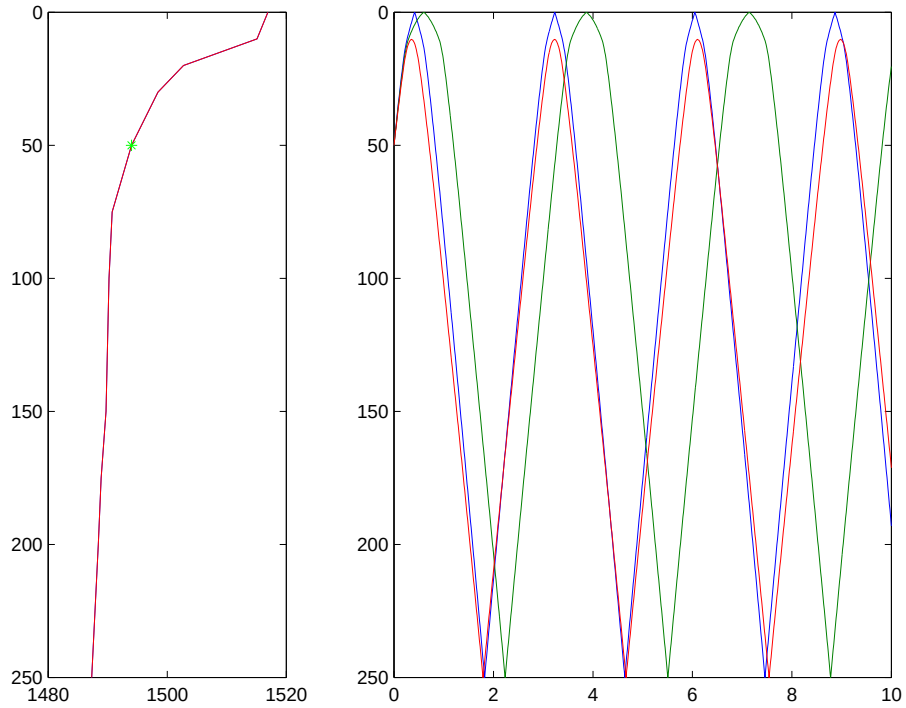

Figure 14 *Sound speed profile (SwellEx-96) and rays propagating with an initial angle of −10.5 (blue) −10 (green) and −9.5 (red) deg. Notice that the cycle skip distance first increases, but then decreases as the shallower ray does not reach into the top layer. [***ray2***]*

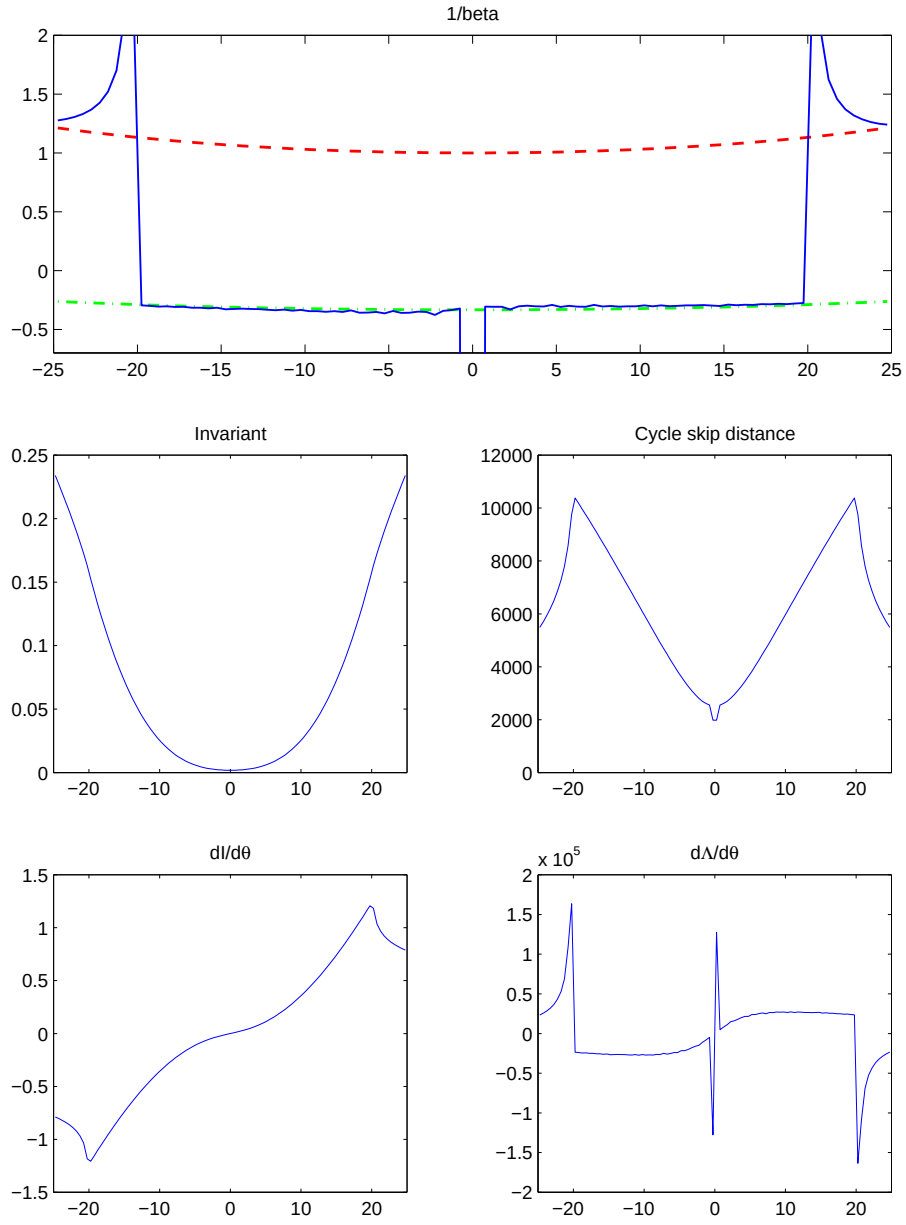

Figure 15 *Computation of β^{-1} for a waveguide with a n^2-linear sound speed varying from 1450 to 1550 m/s with the source at 50-m depth. For $|\theta_0| > 20°$ the rays are interacting with both boundaries [***czsq2***]*

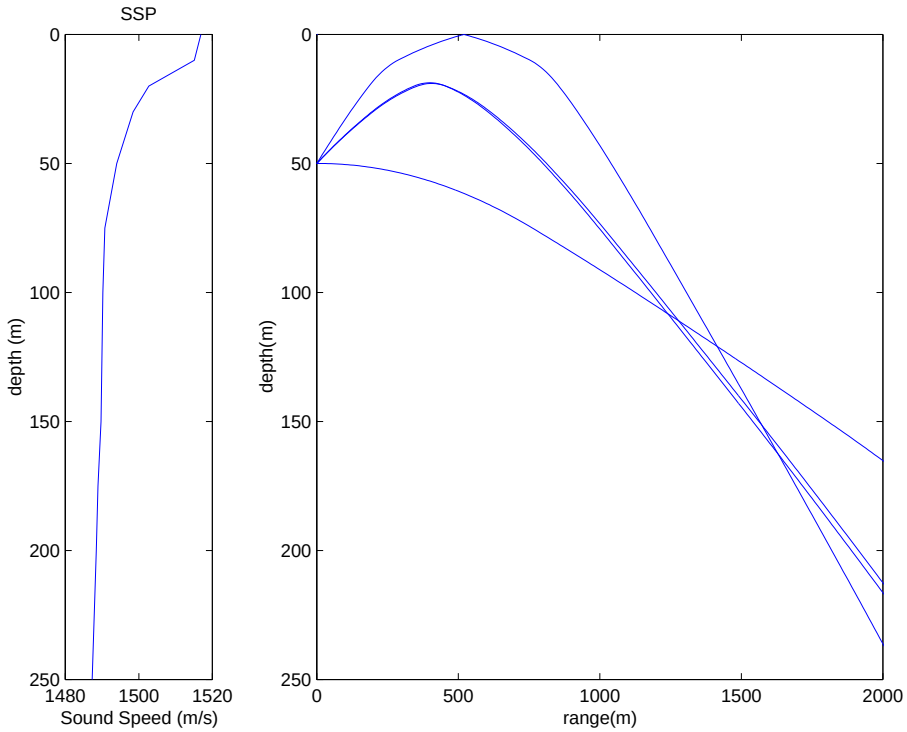

Figure 16 *Sound speed and ray-trace for the SwellEx-96 waveguide.* [**ex2Reverbray**]

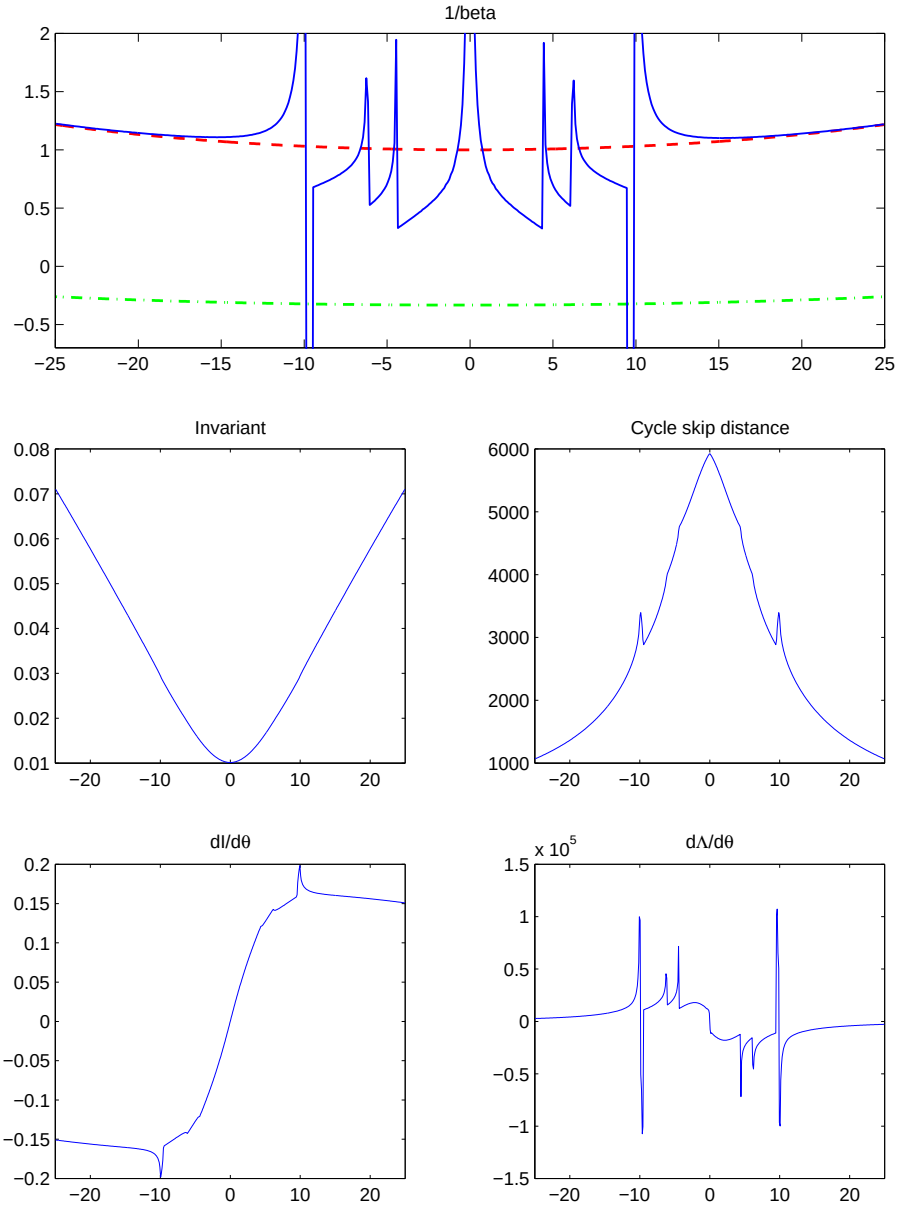

Figure 17 *Beta for the SwellEx-96 waveguide. For reference the* $\beta^{-1} = cos^{-2}\theta_0$ *for a Pekeris wave guide (red dashed) and* $\beta^{-1} = -\frac{1-\tan^2\theta_0}{3}$ *corresponding to the* n^2*-linear profile (green dash-dotted) are shown.* [**ex2Reverb**]

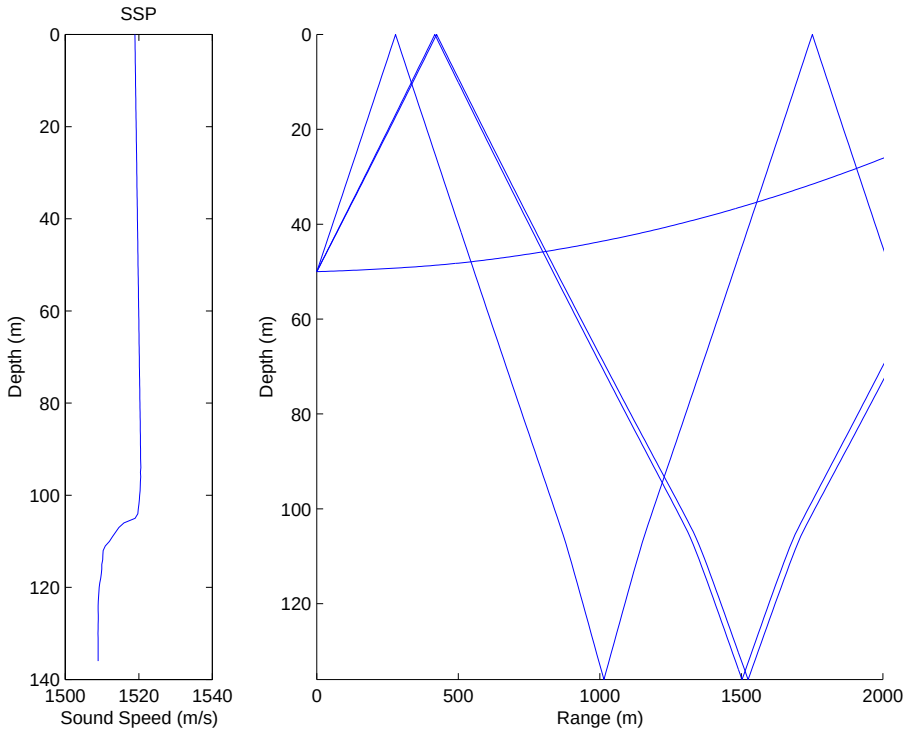

Figure 18 *Sound speed and ray-trace for the* MAPEX2K *(Elba, Nov.2000) waveguide.* [**bmapexray**]

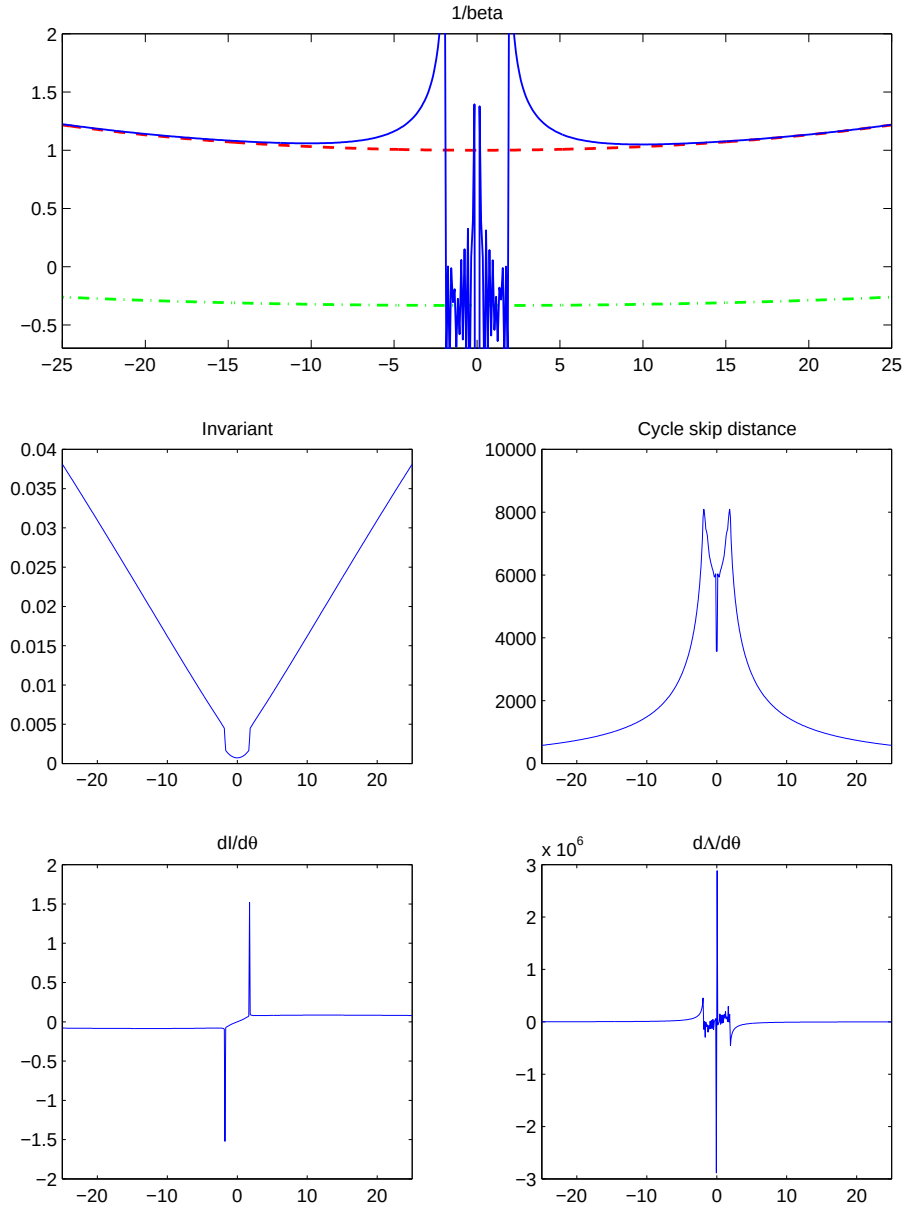

Figure 19 *Beta for the* MAPEX2K *(Elba, Nov. 2000) waveguide. For reference the* $\beta^{-1} = cos^{-2}\theta_0$ *for a Pekeris wave guide (red dashed) and* $\beta^{-1} = -\frac{1-\tan^2\theta_0}{3}$ *corresponding to the* n^2*-linear profile (green dash-dotted) are shown.* [**bmapex**]

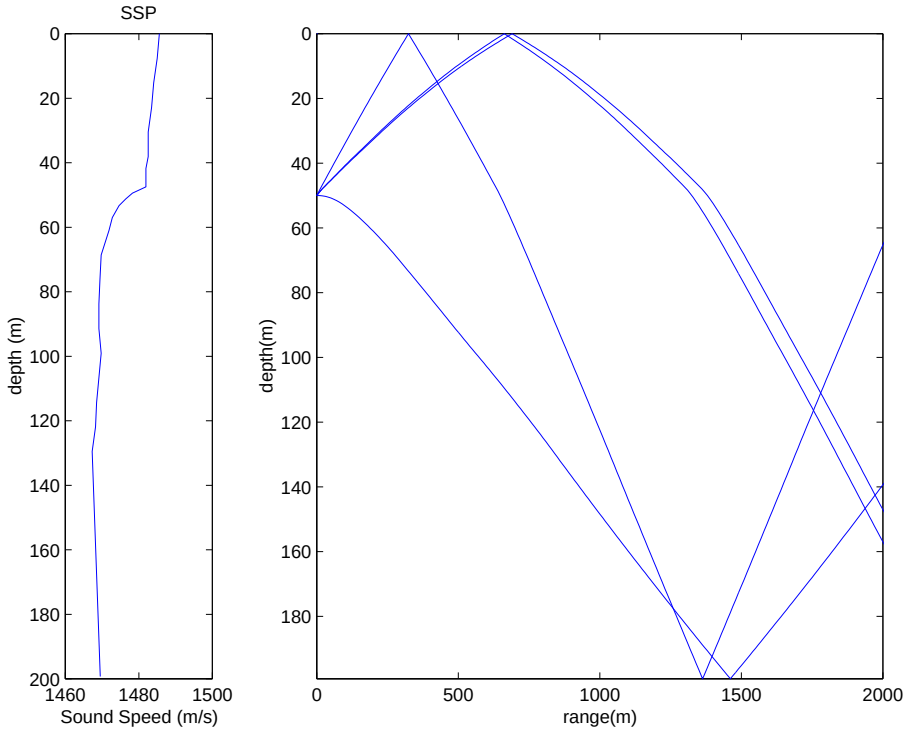

Figure 20 *Sound speed and ray-trace for the Arctic waveguide.* [**geraldexray**]

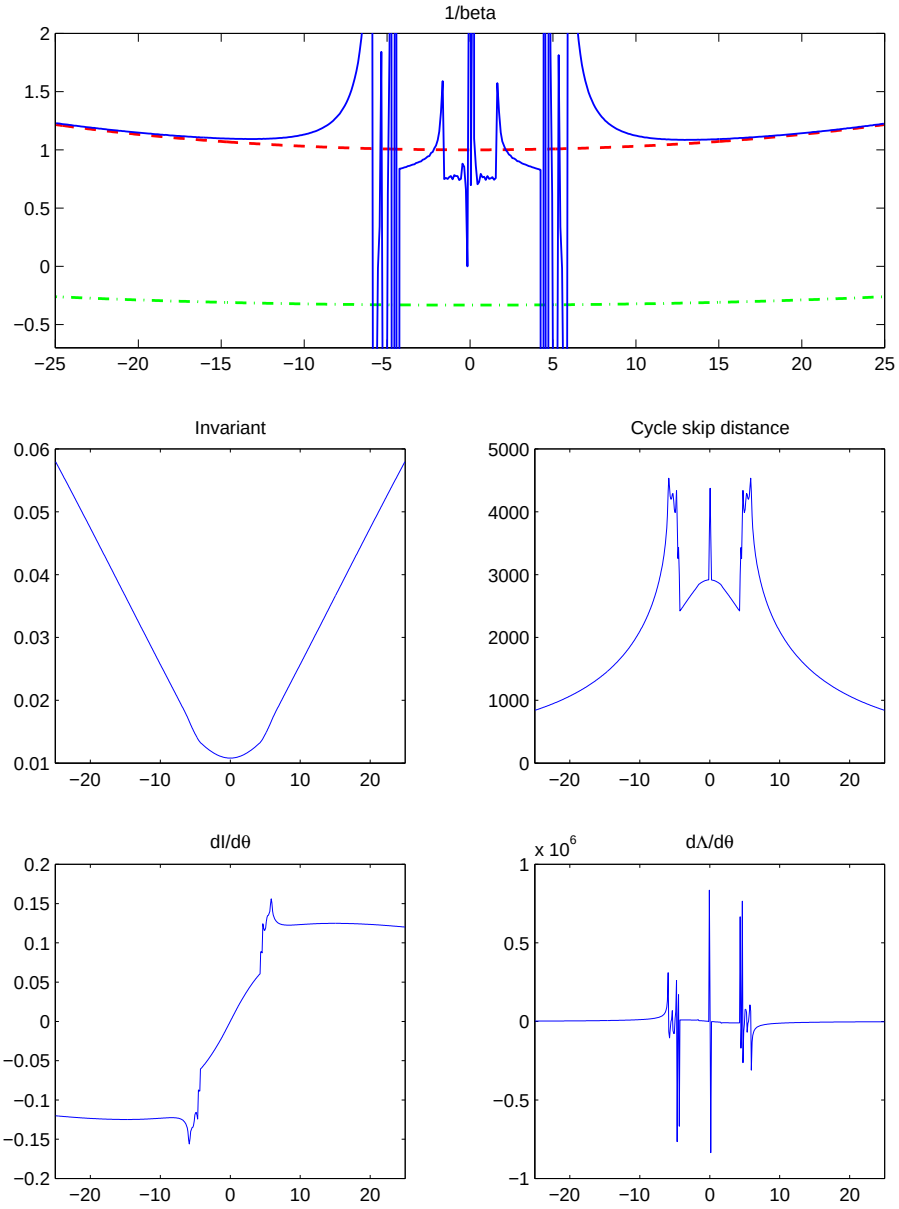

Figure 21 *Beta for the Arctic waveguide. For reference the* $\beta^{-1} = cos^{-2}\theta_0$ *for a Pekeris wave guide (red dashed) and* $\beta^{-1} = -\frac{1-\tan^2\theta_0}{3}$ *corresponding to the* n^2*-linear profile (green dash-dotted) are shown.* [**geraldex**]

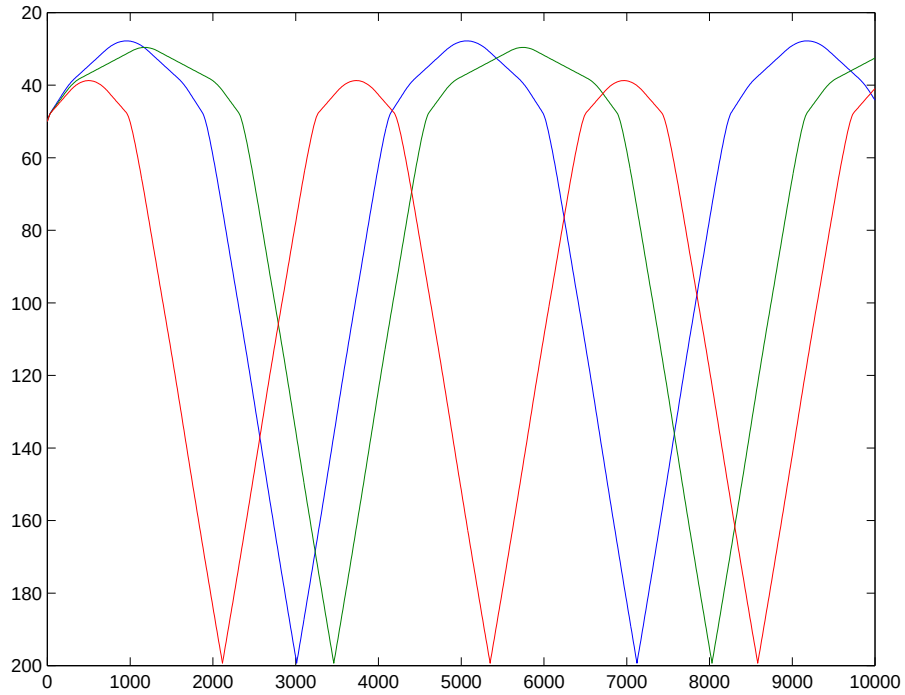

Figure 22 *Ray-trace for the Arctic waveguide for a launch angle of* $-4.8°$ *(blue)* ,$-4.7°$ *(green) and* $-4.6°$ *(red). Notice how the cycle skip distance first increase (blue to green) and then drastically decreases (green to red).* [**geraldexmoreray**]

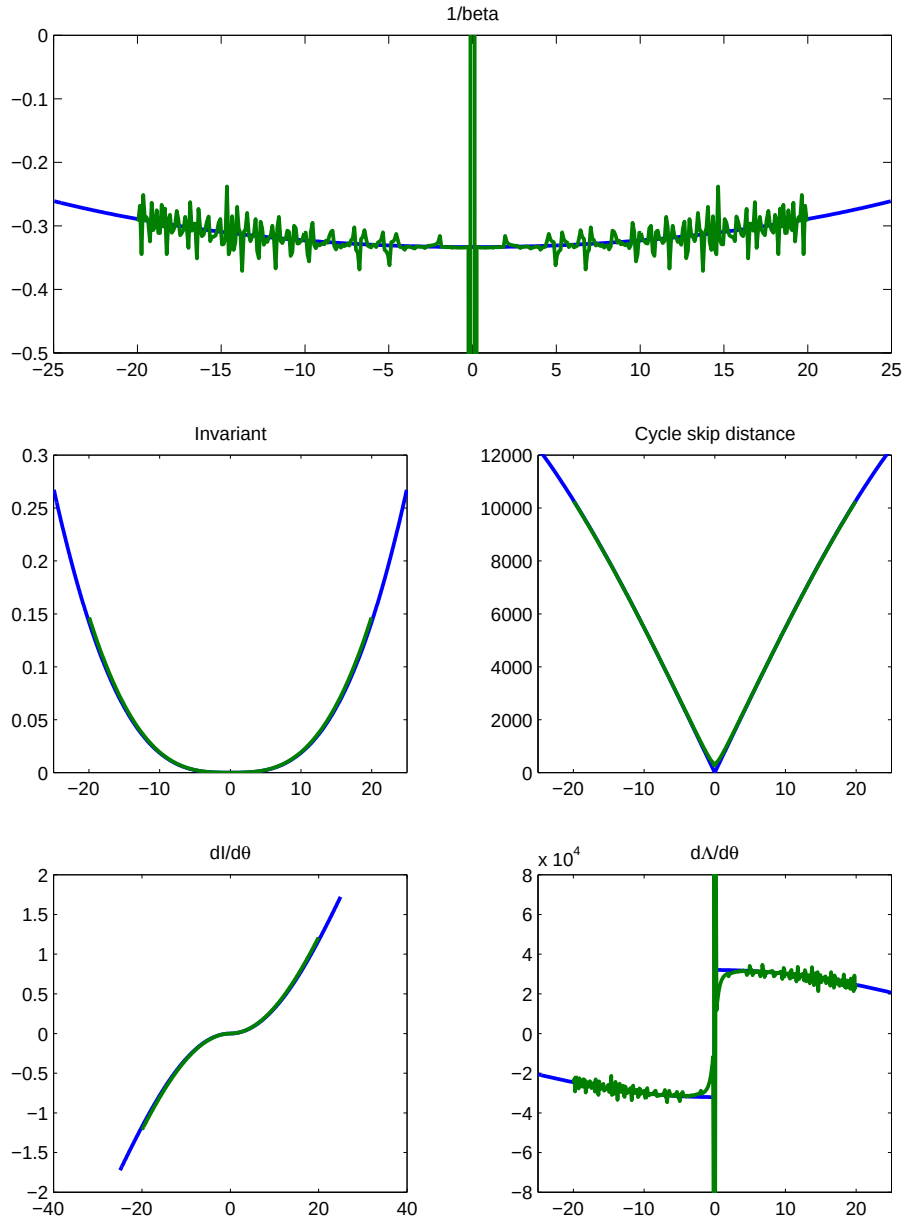

Figure 23 *Beta based on CASS/GRAB raytracing. The sound speed was a 1000-m deep n^2-linear profile from 1500 to 1450, approximated every 10 m. Analytic (blue) Peters matlab (green). The launch angle increment is* 0.1°. *[***czsqana01***]*

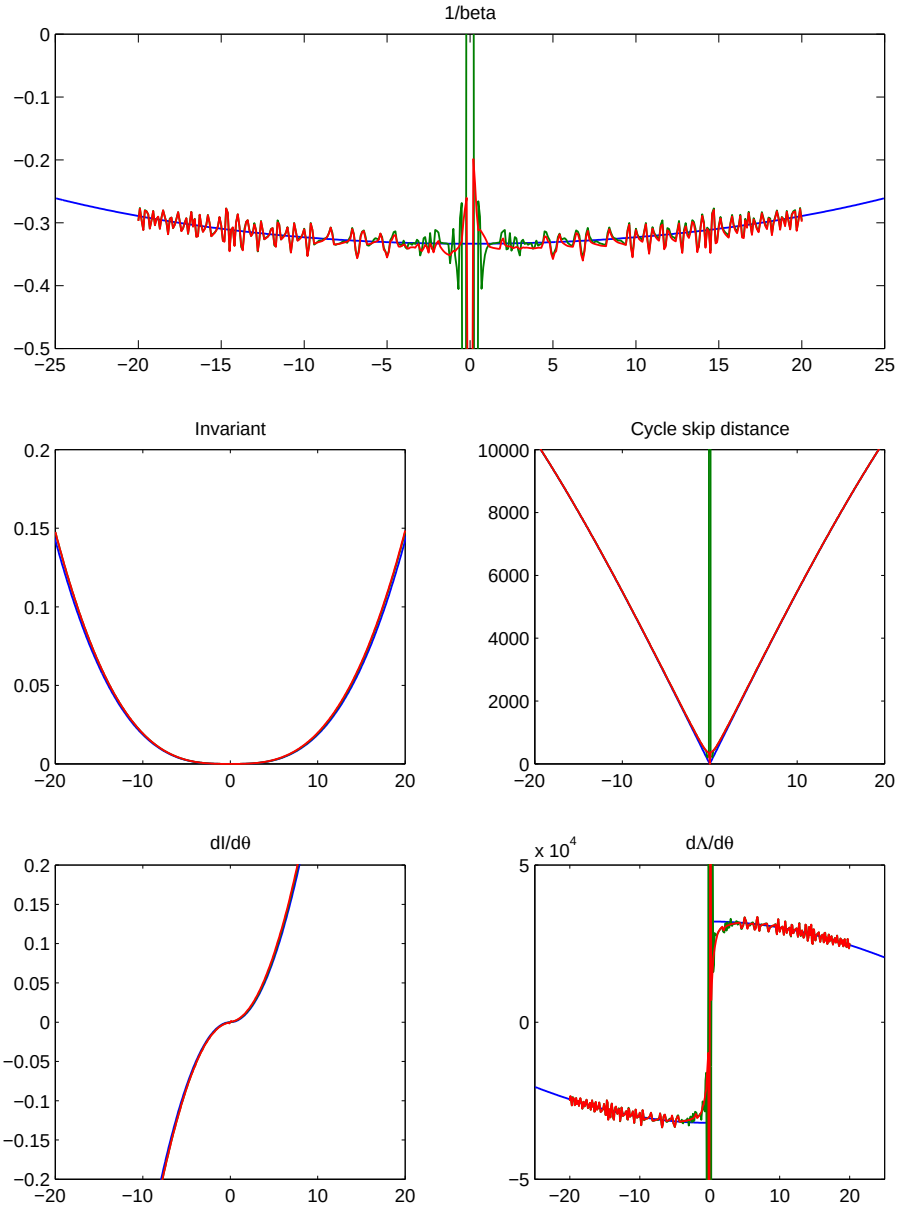

Figure 24 *Beta based on bellhop raytracing. The sound speed was a 1000-m deep n^2-linear profile from 1500 to 1450, approximated every 10 m. Analytic (blue) Peters matlab (green) and Mike's matlab(red). The launch angle increment is* 0.1°. *[***czsqanabell***]*

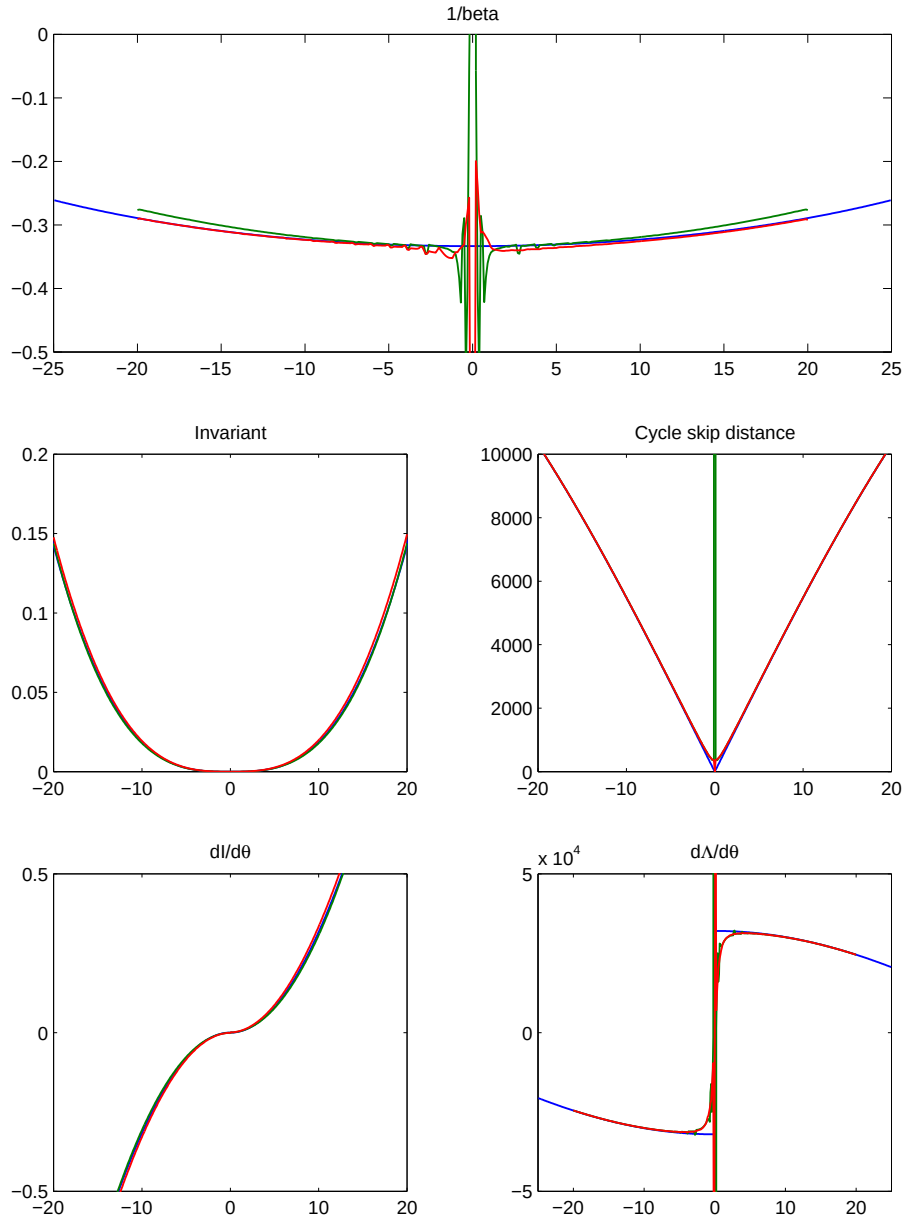

Figure 25 *Beta based on bellhop raytracing. The sound speed was a 1000-m deep n^2-linear profile from 1500 to 1450, using option N in Bellhop. Analytic (blue) Peters matlab (green) and Mike's matlab(red). Peters matlab deviates slightly as it does linear interpolation between sound speed points.* **[czsqana2]**

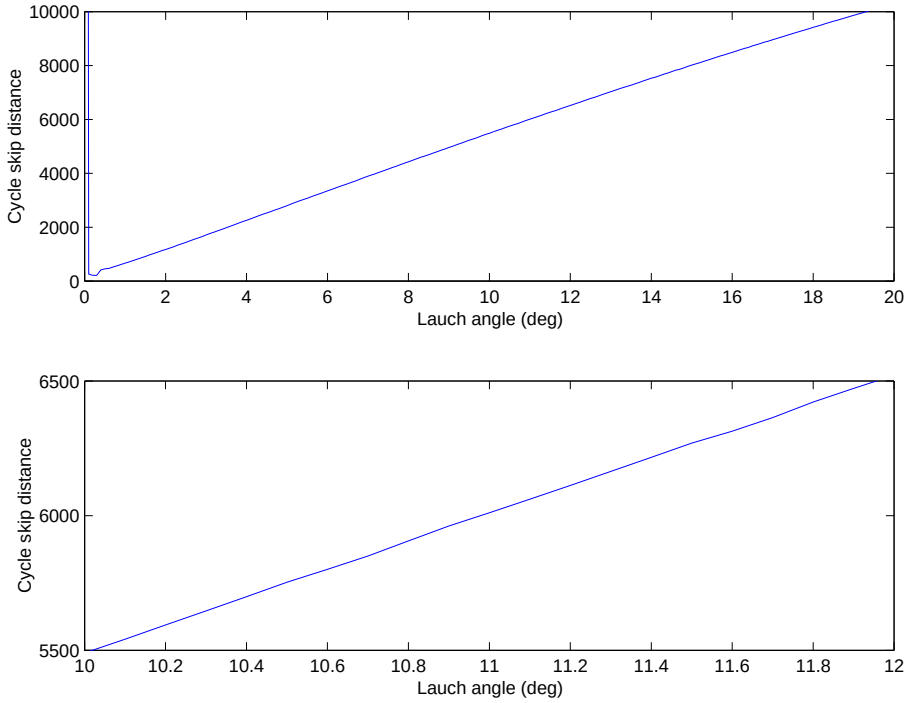

Figure 26 *Cycle distance calculated for bellhop using the sound speed for a 1000-m deep n^2-linear profile from 1500 to 1450, approximated every 10 m. The launch angle increment is* $0.1°$. *[***czsqcycle***]*

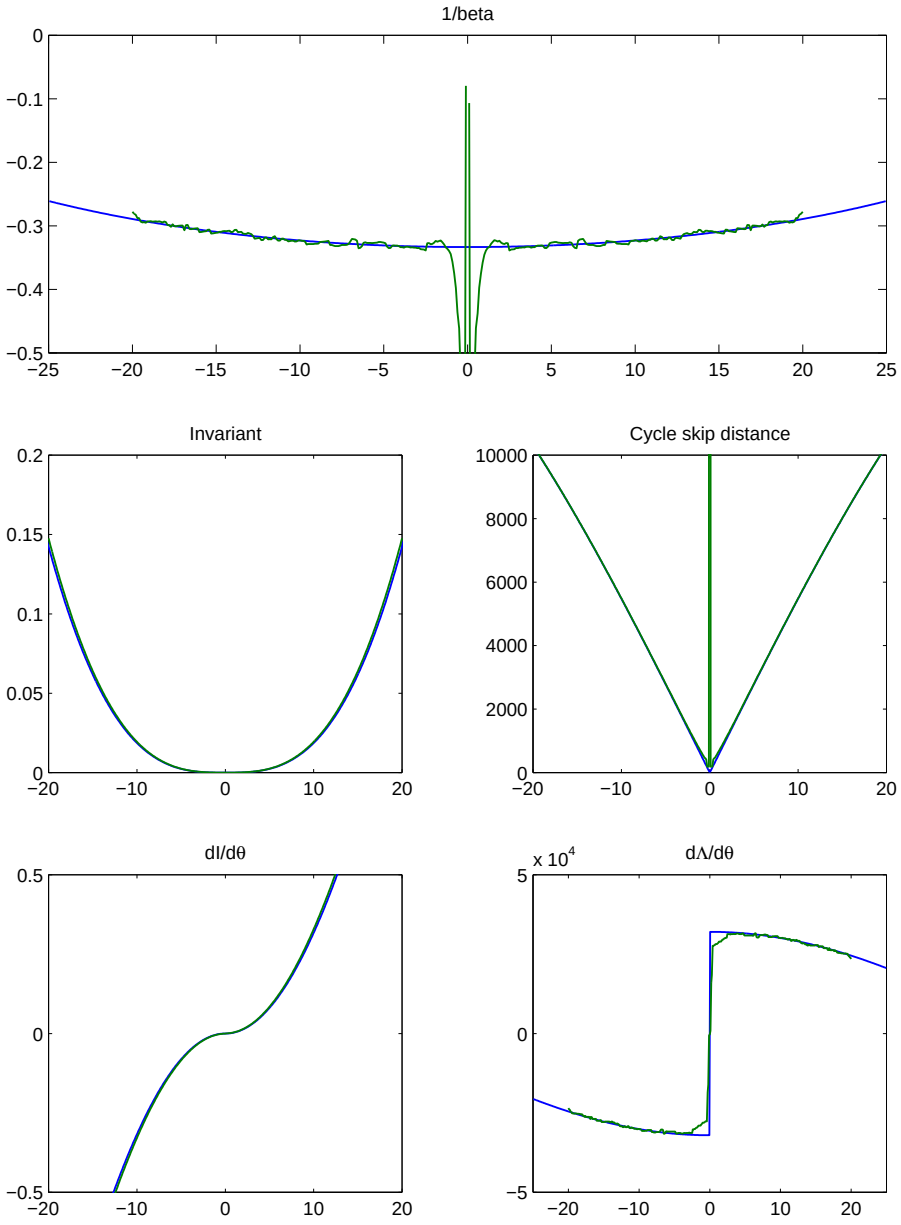

Figure 27 *Beta based on bellhop raytracing. Analytic (blue) Peters matlab (green) with a 11-point median filtering of the cycle skip distance. The launch angle increment is* 0.1°. *[***czsqanabellmed***]*

Annex A
MPL CASS unix installation

The MPL CASS [4, 6, 5, 7] installation is based on version 2 as that was already ported to UNIX by APL/Washington and the changes in version 3 seem minimal for most applications.

A.1 Directories

cass root directory.
cass/cassv3 contains CASS version 3 (documentation source code and examples.
mail Correspondence for obtaining CASS
unixcass The source code and present installation.
mplExamples Examples used to generate the examples in the report.
beta This document.
oldExamples Older CASS examples and APL examples. It is not recommended to use these. Rather use the examples in `cassv3/`, See sect. A.5

A.2 Installation of CASS

To install GRAB/CASS:
```
cd ~/cass/unixCass/
make
```

CASS compiles using either Sun's f77 or Gnu g77 (with f77 as default).

Include CASS in your `path`:
```
set path = ($path ~/cass/unixCass/bin/ )
```

A.3 Running CASS

A standard CASS/GRAB input file is *.input and output *.output

To run CASS/GRAB
```
cass filename
```

The standard plotting for CASS is based on the old DISSPLA plotting program (it is available from Computer Associates for about 6000 USD). To get a real production code the plotting is needed. However, all output can also be printed to the *.output file and the data for the plots can then be extracted using either cut-and-paste for new plots or searching for specific strings (e.g. with *sed*).

For some standard plots this has already been automated (see below), but for many of the advanced options available in CASS the data must be extracted from the output file using cut-and paste and then plotted using e.g. Matlab.

It is suspected that the PC-version has the plotting embedded and therefore is more user friendly. It is not clear if MPL has all software to run the standard PC-version.

For the standard plots produced here this is done by running the postprocessor:
`casspost.scr filename`

This script extracts sound speed, ray diagram and reverberation data from the output to separate files, so that they can be plotted.

The execution and plotting of CASS is controlled by the `runcas.m` matlab file. An example is in `/cass/mplExamples/working`.

A.4 Documentation

A user manual is available in `cass/cassv3/`.

There is a CASS (directory `cass/cassv3/cass_sdd`) and a GRAB `cass/cassv3/grab_sdd`) software description description. These are only interesting for the software developer or for very technical personnel.

The user can find helpful examples from the standard test descriptions (directory `cass/cassv3/cass_std and cass/cassv3/grab_std`).

A.5 Examples

Most of CASS's calculations are based on a successful GRASS (ray-tracing) run. Thus the first step in doing calculations is to assure that the ray-tracing is done correctly. The user should always first examine the ray-trace diagram.

Examples for the *Standard Test Description* are provided in the subdirectories of the documentation. Because these are made for the PC-version and are from a different CASS version they usually need some minor editing before they will run.

There is also some examples in the `/oldexamples/cass` directory. They are not documented. They usually need some minor editing before they will run.

Some advanced examples from APL/Washington, based on the unix version, are available in the `/oldExamples/aplExamples/` directory.

Finally, the MPL examples are available in the `mplExamples/` directory.